Physics – Uspekhi **55** (10) 1035 – 1058 (2012)

CONFERENCES AND SYMPOSIA

PACS numbers: 01.10.Fv, 33.50.Dq, 42.50.Nn, 42.55.Ah, 42.70.Nq, **71.45.–d**, 73.20.Mf, **73.22.–f**, 78.20.Ek, 78.67.Bf, 78.67.Pt, 81.05.Xj

Plasmonics
(Scientific session of the Physical Sciences Division of the Russian Academy of Sciences, 21 February 2012)

DOI: 10.3367/UFNe.0182.201210g.1111

A scientific session of the Physical Sciences Division of the Russian Academy of Sciences (RAS), entitled 'Plasmonics', was held in the Conference Hall of the Lebedev Physical Institute, RAS on 21 February 2012.

The following reports were put on the session agenda posted on the website www.gpad.ac.ru of the RAS Physical Sciences Division:

(1) **Kukushkin I V, Murav'ev V M** (Institute of Solid State Physics, RAS, Chernogolovka, Moscow region) "Terahertz plasmonics";

(2) **Lozovik Yu E** (Institute of Spectroscopy, RAS, Troitsk, Moscow region) "Plasmonics and magnetoplasmonics based on graphene and a topological insulator";

(3) **Protsenko I E** (P N Lebedev Physical Institute, RAS, Moscow) "Dipole nanolaser";

(4) **Vinogradov A P, Andrianov E S, Pukhov A A, Dorofeenko A V** (Institute for Theoretical and Applied Electrodynamics, RAS, Moscow), **Lisyansky A A** (Queens College of the City University of New York, USA) "Quantum plasmonics of metamaterials: loss compensation using spasers";

(5) **Klimov V V** (Lebedev Physical Institute, RAS, Moscow) "Quantum theory of radiation of optically active molecules in the vicinity of chiral nano-meta-particles".

The papers written on the basis of oral reports 2–5 are published below.

PACS numbers: **71.45.–d**, 73.20.Mf, **73.22.–f**
DOI: 10.3367/UFNe.0182.201210h.1111

Plasmonics and magnetoplasmonics based on graphene and a topological insulator

Yu E Lozovik

Plasmonics is one of the most rapidly developing interdisciplinary branches of physics. From the fundamental point of view, plasma oscillations in solids comprise collective oscillations of electron gas density controlled by Coulomb electron interaction; in the simplest case, the oscillation dispersion law is defined by the electron concentration in the conduction band, the permittivity of the medium (of the crystal without the inclusion of conduction electrons), and their effective mass. In the general case, for instance, for interband plasmons, the plasmon dispersion law depends on the electron band structure. The damping of plasma oscillations is determined both by single-particle mechanisms of carrier scattering by impurities, etc. and by Landau damping. In microscopic terms, the latter corresponds to the decay of a plasma oscillation quantum — a plasmon — into two single-particle excitations: an electron and a hole. To state it in macroscopic terms, as shown by Ginzburg, this decay constitutes an inverse Vavilov–Cherenkov effect (electron acceleration by the field of a plasma wave). Plasmon excitation, for instance, with the help of characteristic electron losses was employed for the description of solids (see Refs [1–3] and references cited therein).

Plasmonics emerged from the study of plasmons in low-dimensional systems and structures and from the development of their applications. The specific character of (surface and local) plasmons in these systems consists in the fact that the frequency and damping of plasmons in them is defined by the geometry of the structure and the permittivity of the environment, because the lines of force of the Coulomb fields of the interacting electrons also pass through the ambient medium [4–7]. The last circumstance may be used for creating supersensitive plasmon sensors (see Ref. [8] and references cited therein). Plasmon excitation is widely used in surface spectroscopy [9, 10], and local plasmon excitation is employed for a giant enhancement of Raman light scattering [11] and of different nonlinear optical processes (see, for instance, Ref. [12] and references cited therein). It would be instructive to produce a complete set of control elements for two-dimensional, surface plasmon optics (plasmon mirrors, lenses, etc.). The feasibility of realizing time-resolved surface plasmon optics has also been discussed, and the first successful steps in this direction have been reported [13, 14]. The excitation of local plasmons on the tip of a scanning probe microscope by an incident electromagnetic wave may be employed for producing under the tip a subwavelength domain with a strongly enhanced field; this, in turn, was used for local spectroscopy and nanolithography with an ultrahigh spatial resolution which far exceeded the Rayleigh limit (see Refs [15–17] and references cited therein).

Another possible application of plasmons and plasmon polaritons is ultrafast information transfer (for instance, between the elements of a chip), faster than with electron current pulses. Lastly, an interesting possibility consists in the

Yu E Lozovik Institute of Spectroscopy, Russian Academy of Sciences, Moscow, Russian Federation; Moscow Institute of Physics and Technology, Dolgoprudnyi, Moscow region, Russian Federation
E-mail: lozovik@isan.troitsk.ru

Uspekhi Fizicheskikh Nauk **182** (10) 1111 – 1135 (2012)
DOI: 10.3367/UFNr.0182.201210g.1111
Translated by E N Ragozin; edited by A Radzig

Uspekhi Fizicheskikh Nauk **182** (10) 1111 – 1116 (2012)
DOI: 10.3367/UFNr.0182.201210h.1111
Translated by E N Ragozin; edited by A Radzig

development of quantum plasmonics for quantum informatics, etc.

All these promising applications are significantly limited by the damping of plasmons — by their finite mean free path. This impediment can be overcome with the aid of active plasmonics by using spasers — plasmon analogs of lasers [18–20]. In particular, it will be possible by using a spaser in the form of the tip of a scanning probe microscope and measuring the loss-induced dips in its generation spectrum to realize supersensitive spectroscopy with an ultrahigh spatial resolution [21], which represents, in a sense, a spaser analog of selective near-field laser spectroscopy [22]. This method may also be utilized for the supersensitive spaser spectroscopy of surfaces [23]. Spasers are also the concern of reports to this session of the Physical Sciences Division of the RAS [24, 25].

Another method of overcoming the specified difficulty involves the search for and use of radically new systems with a weak plasmon damping like doped graphene. Below, we briefly discuss the collective electronic and optical properties of graphene and topological insulators, which were analyzed in our work.

From the fundamental standpoint, the keen interest in graphene — a single isolated plane of graphite, which is stable even without a substrate (see reviews [26–35] and references cited therein) — and in recently discovered (three-dimensional) topological insulators (see reviews [36, 37] and references cited therein) is due to the fact that in these entirely different materials — graphene and topological insulator surfaces — there is a two-dimensional electron gas with a zero effective mass and a zero gap between the conduction and valence bands. This two-dimensional electron gas is described by the Dirac equation with a zero mass (as for neutrinos!), and therefore one may draw an analogy to ultrarelativistic physics of elementary particles and quark matter. This leads to a number of interesting effects comprising the absence of backward reflection from potential barriers at normal incidence (Klein tunneling), weak antilocalization, and the half-integer quantum Hall effect (observable even at room temperature!).

A difference from ultrarelativistic particle physics must also be emphasized: in the Dirac equation for graphene, in place of the speed of light a quantity 300 times lower appears, and this equation is valid only in the laboratory frame of reference (because in the derivation of the effective Dirac equation for graphene they proceed from the Galilean-invariant Schrödinger equation).

Certainly, it should be remembered that these are the so-called envelopes obeying the Dirac equation in an external field. These envelopes describe the slow modulation (due to slowly varying external fields) of Bloch functions which oscillate with a lattice period (used in this case is the adiabatic approximation which leads for ordinary crystals to the Schrödinger equation with an effective mass).

The linear dispersion law for graphene was first established [38, 39] proceeding from the Schrödinger equation which took into account the symmetry and the existence of two sublattices in graphene, within an approximation accounting for the closest neighbor interaction. But this linear spectrum (valid up to an energy on the order of 1 eV), i.e. the presence of Dirac-effective electrons, is associated, as may be shown, with the symmetry of graphene, and this property is protected from the presence of impurities and some other perturbations by symmetry with respect to time reversal. The role of spin in the Dirac equation is played by pseudospin which emerges due to the fact that the hexagonal lattice in graphene may be represented in the form of two equivalent triangular lattices displaced relative to each other. The presence of two more components in the Dirac equation for graphene is associated with the existence of two independent valleys in the Brillouin zone for graphene (since the existence of two sites in the graphene elementary cell results in two sites in the elementary cell of the reciprocal lattice).

The interest in graphene, of course, is spurred by the prospect of numerous applications related to its unique properties. Graphene is one atom thick, so that an extremely small size as a possible element of nanoelectronics or optoelectronics is reached in one dimension. It is valid to say that a new class of materials made its appearance owing to the discovery of graphene — two-dimensional membranes stable even without a substrate. Graphene is compatible with the traditional technology of the planar nanostructure production (unlike, for instance, nanotubes). It may posses a high electron mobility even at room temperature, and its thermal conductivity is significantly higher than that of copper. Furthermore, the intrinsic strength of graphene is 200 times greater than the strength of steel. Owing to these remarkable properties, graphene shows promise for making coatings of solar batteries and screens, new composite nanomaterials, ultracapacitors, and nanoelectronic elements.

An interesting property of graphene consists in the possibility of changing its transport characteristics upon adsorption of molecules, etc., which opens the prospect of making supersensitive nanosensors on its basis.

An important property of graphene is the possibility of easily controling the density of electrons or holes with the help of external control electrodes (or external chemical doping).

Such a property may be employed for transistors, though only for analog transistors, not digital ones. This is due to the absence of an energy gap in graphene, because there is no way of blocking the electric current in digital transistors. However, opening the gap with the aid of geometrical quantization — by using graphene tapes or bigraphene in a transverse electric field — will permit the employment of such systems in digital transistors as well. The application of concentration guiding with control electrodes in a bilayer graphene system was proposed for making a system of two separated layers of Dirac electrons and holes of equal concentrations. Possible in this system is the Bose–Einstein condensation (BEC) of dipole pairs or excitons from spatially separated electrons and holes in a magnetic field [40–42] (which exist in graphene only in a magnetic field owing to the absence of backward reflection of electrons) or their Bardeen–Cooper–Schrieffer (BCS) type pairing (see Refs [43–52]) due to Coulomb attraction (similar to the pairing in a three-dimensional excitonic insulator [53, 54]), which leads to the appearance of undamped electric currents in each of the layers in the system under consideration. The difference between a graphene bilayer and a bilayer of paired electrons and holes with a nonzero mass [55] consists in the absence of the ordinary BEC–BCS crossover (without a magnetic field) upon lowering the pairing particle concentration and the existence of an angular factor associated with the spinor nature of the Dirac wave function, the factor which suppresses backward scattering. The system considered here may be utilized as a dissipation-free information transfer line. A similar system of spatially separated Dirac electrons and holes and their pairing and superfluidity may be realized by independent doping with the help of independent control electrodes for the opposite surfaces of the superthin film of a

topological insulator (see Ref. [56] and references cited therein). Heavy doping may give rise to intrinsic superconductivity in graphene (see Ref. [57] and references cited therein).

The specific character of the graphene's band structure results in interesting features of its dielectric response: to the existence of a singularity in the low-frequency range (like for a metal, though weaker), to highly unusual optical properties [58], and to a weak damping of quasiparticles in it. These properties show good promise of making photonic crystals on the base of graphene which has a photonic gap in the far-infrared spectral region hardly blurred by damping (unlike that in metals) [59].

The possibility of controling the electron concentration in graphene with the aid of control electrodes opens the door to graphene-based plasmonics [60–64]. In particular, it is possible to make plasmon waveguides and plasmon switches using the specially profiled coatings and control electrodes on graphene. Critically important additional virtues of graphene for plasmonics are a weak damping, a long mean free path of plasmons in it, and the capability of working in the terahertz frequency range. The weak damping opens the way for the development of a graphene-based quantum plasmonics or single-plasmonics.

It will be of interest to control plasmons in graphene and nanomaterials based on it with the help of an external magnetic field (see Ref. [62] and references cited therein). We analyzed the properties of polaritons in an optical microcavity with graphene embedded into it (Fig. 1) and their properties in the terahertz frequency range [63, 64]. We also considered the TE and TM modes in graphene which borders on two adjacent media with a low dielectric contrast between them. In the frequency range where the imaginary part of the permittivity is small, the properties of the system turned out to be critically dependent on the low dielectric contrast between the media. This leads to a leakage of surface waves, which permits making an ultrahigh-sensitivity sensor on the base of this system [65].

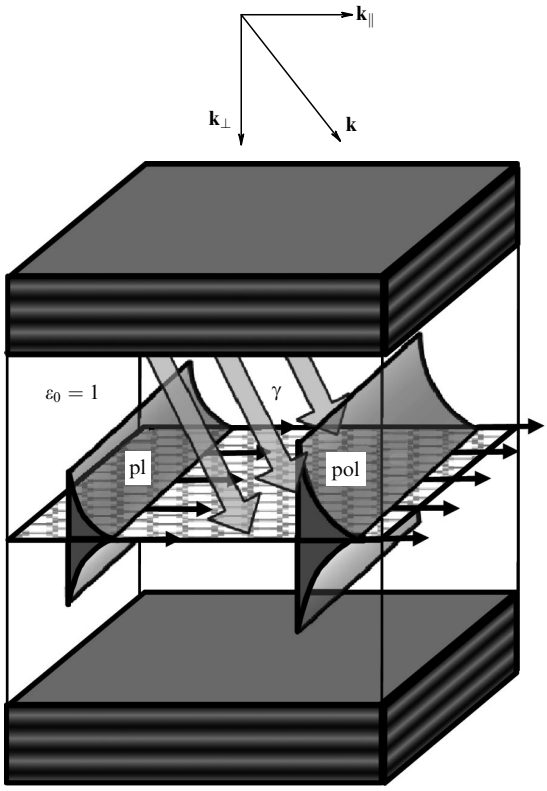

Figure 1. Polariton (pol) in an optical microcavity wherein graphene is embedded; pl is a plasmon, and γ is a photon.

Also of interest is the possibility of controling collective excitations in graphene as well as polaritons in an optical microcavity, which graphene is embedded in, with the aid of Coulomb drag by the electron current in the graphene-neighboring layer of two-dimensional electron gas in a quantum well [66].

As noted above, Dirac electrons exist not only in graphene, but also on the surfaces of recently discovered new materials — three-dimensional topological insulators [36, 37]. To date, the two- and three-dimensional realizations of topological insulators have been studied. The new paradigm is that topological insulators are not connected with the emergence of spontaneous symmetry breaking in a crystal and, in turn, with its attendant order parameter (as in the case, for example, of magnetics, ferroelectrics, etc.), but with the emergence of a topological invariant in Hilbert space, which is determined by the properties of the Bloch states occupied by electrons. In this sense, there is an analogy between the properties of topological insulators and the quantum Hall effect in which none of the states in the plateau region inside the system are conductive, but at the system boundary there are zero-gap chiral states (a unidirectional current determined by the direction of the magnetic field) protected from the influence of impurities, etc. by the existence of a topological invariant in Hilbert space. This picture is especially simple in sufficiently strong magnetic fields, where the drift approximation applies to electrons and the topological invariant has a simple meaning: it characterizes the connectivity of drift electron trajectories [67]. In three-dimensional (so-called strong) topological insulators, there is a gap in the spectrum of bulk states, as in ordinary insulators, but on the surface they have, owing to the existence of the topological invariant, zero-gap surface electron states with zero effective masses of electrons and holes (as in graphene), which are described by the Dirac equation with a zero mass.

These states are topologically protected: ordinary, non-magnetic impurities cannot form a gap and localize these states owing to the presence of a topological invariant. One of the important properties of the Dirac equation with a zero mass is a strict connection between the directions of electron momentum and spin (of momentum and pseudospin for graphene).

Owing to a strong spin-orbit interaction, electrons on the surface of a topological insulator possess a strict correlation between the spin and momentum directions: their spin is perpendicular to the momentum, and this property was experimentally revealed by angle- and spin-resolved photoelectron spectroscopy. A similar strict connection between electron momentum and pseudospin (and not spin!) is true for graphene owing to the mathematical equivalence of the Dirac equations with a zero mass for both systems, which this connection follows from.

This connection leads, in particular, to unusual properties of plasmons on the surface of topological insulators (see Refs [68–70]). In quantum terms, a plasmon may be represented as a coherent superposition of excited pairs of electrons and holes shifted in momenta, which correspond for

doped graphene to both intraband ($\gamma = \gamma'$) and interband ($\gamma \neq \gamma'$) transitions, so that the plasmon production operator is defined by the linear superposition of the electron production and annihilation operators:

$$Q_{\mathbf{q}}^{+} = \sum_{\mathbf{p}\gamma\gamma'} C_{\mathbf{pq}}^{\gamma'\gamma} b_{\mathbf{p}+\mathbf{q}\gamma'}^{+} b_{\mathbf{p}\gamma} ,$$

where **p** and **q** are the two-dimensional momenta.

The plasmon dispersion law can be found by way of linearization of the equations of motion for Dirac electrons, which corresponds to a random phase approximation. The validity of the random phase approximation is defined by the dimensionless quantum parameter equal to the ratio between the characteristic energy of Coulomb interaction and the quantum kinetic energy. For Dirac electrons with a linear dispersion law, this ratio is independent of the electron concentration and is equal to the effective fine-structure constant in which the speed of light is replaced by the electron velocity entering into the Dirac equation for a topological insulator (and graphene), and the charge squared is divided by the permittivity of the surrounding medium. This permittivity is high for topological insulators, and the random phase approximation, therefore, holds true.

Related to the preferential value of plasmon momentum is the preferential momentum of the electrons and holes, which define the plasmon production operator. Because of the strict momentum–spin connection for Dirac electrons, preferential spin emerges as well. Thus, a plasma wave in a topological insulator is always associated with a spin wave! Moreover, an uncompensated total spin polarization emerges in the production of a plasmon (Fig. 2). In the scattering of a spin-plasmon by the nonuniformities of an electric or magnetic field, the angular diagram turns out to be strongly anisotropic and consists of two lobes (Fig. 3).

Interesting effects occur when a magnetic impurity layer or a film of magnetic material is deposited onto the surface of a topological insulator. The external exchange interaction (noninvariant with respect to time reversal) of this layer with Dirac electrons induces a gap in the spectrum of the Dirac electrons, and the topological insulator becomes a quantum magnetoelectric: an external electric field induces (apart from the ordinary electric polarization of the volume) a magnetic moment, while a magnetic field induces an electric dipole moment. This gives rise, notably, to appearing quantized nondiagonal Hall conductivity, and therefore to the quantum Faraday and Hall effect — quantized rotations of the polarization plane of transmitted or reflected electromagnetic waves (in the absence of an external magnetic field!). The chiral properties of the system give rise to chiral properties of the excitons inside the topological insulator gap (dependence of the energy on the sign of angular momentum projection). That is why these chiral excitons make a resonance contribution to the nondiagonal conductivity of the system, which may greatly enhance the Faraday effect in comparison with its quantized magnitude (defined only by the fine-structure constant) (see Refs [71, 72] and references cited therein).

The Coulomb field of the electrons located above the surface of a topological insulator with two-dimensional (2D)

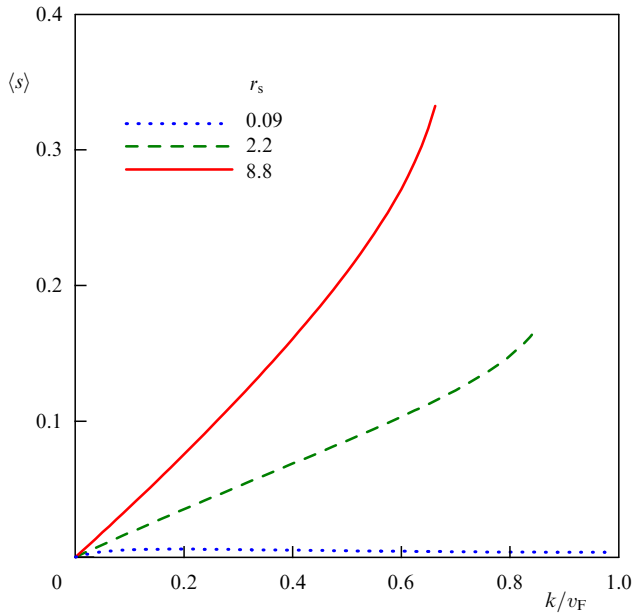

Figure 2. Average value of the spin induced by one plasmon in a two-dimensional Dirac gas on the surface of a topological insulator as a function of its wave vector divided by the Fermi velocity. Parameter r_s is the dimensionless coupling constant for Dirac electrons (the effective fine-structure constant).

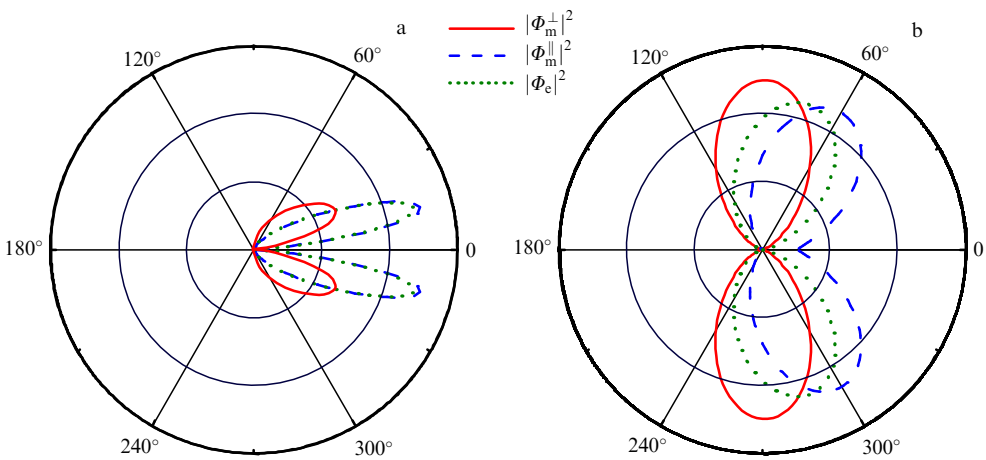

Figure 3. Angular diagram of scattering by nonuniformities of an electric (a) and magnetic (b) field for a spin-plasmon with a momentum $p = 0.2$ (divided by the Fermi velocity). $\Phi_m^{\perp}$, $\Phi_m^{\parallel}$ are the magnetic form factors, and Φ_e is the electric form factor.

chiral electrons induces a magnetic polarization which is equivalent, owing to the symmetry of the problem, to the presence of image magnetic monopoles (similarly to image charges). For a sufficiently dense 2D-electron gas, the emerging total external magnetic field of all the image monopoles may be considered to be uniform and proportional to the surface density of the external electrons and the magnetic monopole charge. This field can manifest itself in the Hall effect for the external electrons and in a change in the dispersion law of their plasma oscillations. For a rarefied system of external electrons, they must exhibit the Aharonov–Bohm effect on magnetic fluxes associated with foreign image monopoles and, therefore, be anions — fractional statistics particles (see paper [73] and references cited therein).

Acknowledgments. This work was supported by the Russian Foundation for Basic Research under grant No. 11-02-00858.

References

1. Keldysh L V, Kirzhnitz D A, Maradudin A A (Eds) *The Dielectric Function of Condensed Systems* (Amsterdam: North-Holland, 1989)
2. Kirzhnits D A *Polevye Metody Teorii Mnogikh Chastits* (Field Theoretical Methods in Many-Body Systems) (Moscow: Gosatomizdat, 1963) [Translated into English (Oxford: Pergamon Press, 1967)]
3. Pines D *Elementary Excitations in Solids* (New York: W.A. Benjamin, 1963) [Translated into Russian (Moscow: Mir, 1965)]
4. Lozovik Yu E, Klyuchnik A V, in *The Dielectric Function of Condensed Systems* (Eds L V Keldysh, D A Kirzhnitz, A A Maradudin) (Amsterdam: North-Holland, 1989) Ch. 5
5. Klimov V V *Nanoplazmonika* (Nanoplasmonics) 2nd ed. (Moscow: Fizmatlit, 2010)
6. Shalaev V M, Kawata S (Eds) *Nanophotonics with Surface Plasmons* (Amsterdam: Elsevier, 2007)
7. Bozhevolnyi S I (Ed.) *Plasmonic Nanoguides and Circuits* (Singapore: Pan Stanford Publ., 2009)
8. Zalyubovskiy S J et al. *J. Opt. Soc. Am. A* **29** 994 (2012)
9. Agranovich V M, Mills D L (Eds) *Surface Polaritons: Electromagnetic Waves at Surfaces and Interfaces* (Amsterdam: North-Holland, 1982) [Translated into Russian (Moscow: Nauka, 1985)]
10. Agranovich V *Excitations in Organic Solids* (Oxford: Oxford Univ. Press, 2009)
11. Kneipp K, Moskovits M, Kneipp H (Eds) *Surface-Enhanced Raman Scattering: Physics and Applications* (Berlin: Springer, 2006)
12. Aiboushev A V et al. *Phys. Status Solidi C* **6** (S1) S162 (2009)
13. Lozovik Yu E et al. *Phys. Lett. A* **276** 127 (2000)
14. Lozovik Yu E et al. *Pis'ma Zh. Eksp. Teor. Fiz.* **75** 551 (2002) [*JETP Lett.* **75** 461 (2002)]
15. Lozovik Yu E, Merkulova S P *Usp. Fiz. Nauk* **169** 348 (1999) [*Phys. Usp.* **42** 284 (1999)]
16. Lozovik Yu E, Klyuchnik A V, Merkulova S P *Laser Phys.* **9** 552 (1999)
17. Lozovik Yu E et al. *Laser Phys.* **9** 564 (1999)
18. Bergman D J, Stockman M I *Phys. Rev. Lett.* **90** 027402 (2003)
19. Protsenko I E et al. *Phys. Rev. A* **71** 063812 (2005)
20. Lisyansky A A et al. *Phys. Rev. B* **84** 153409 (2011)
21. Lozovik Yu E et al., arXiv:1208.3389, to be published
22. Kolesnikov A A, Lozovik Yu E, Merkulova S P *J. Russ. Laser Res.* **31** 469 (2010)
23. Lozovik Yu E et al., to be published
24. Protsenko I E *Usp. Fiz. Nauk* **182** 1117 (2012) [*Phys. Usp.* **55** 1040 (2012)]
25. Vinogradov A P et al. *Usp. Fiz. Nauk* **182** 1123 (2012) [*Phys. Usp.* **55** 1046 (2012)]
26. Geim A K *Usp. Fiz. Nauk* **181** 1284 (2011); *Rev. Mod. Phys.* **83** 851 (2011)
27. Novoselov K S *Usp. Fiz. Nauk* **181** 1299 (2011); *Rev. Mod. Phys.* **83** 837 (2011)
28. Castro Neto A H et al. *Rev. Mod. Phys.* **81** 109 (2009)
29. Katsnelson M I *Mater. Today* **10** (1 – 2) 20 (2007)
30. Das Sarma S et al. *Rev. Mod. Phys.* **83** 407 (2011)
31. Kotov V N et al. *Rev. Mod. Phys.* **84** 1067 (2012)
32. Morozov S V, Novoselov K S, Geim A K *Usp. Fiz. Nauk* **178** 776 (2008) [*Phys. Usp.* **51** 744 (2008)]
33. Lozovik Yu E, Merkulova S P, Sokolik A A *Usp. Fiz. Nauk* **178** 757 (2008) [*Phys. Usp.* **51** 727 (2008)]
34. Abergel D S L et al. *Adv. Phys.* **59** 261 (2010)
35. Katsnelson M I *Graphene: Carbon in Two Dimensions* (Cambridge: Cambridge Univ. Press, 2012)
36. Hasan M Z, Kane C L *Rev. Mod. Phys.* **82** 3045 (2010)
37. Qi X-L, Zhang S-C *Rev. Mod. Phys.* **83** 1057 (2011)
38. Wallace P R *Phys. Rev.* **71** 622 (1947)
39. Slonczewski J C, Weiss P R *Phys. Rev.* **109** 272 (1958)
40. Berman O L, Lozovik Yu E, Gumbs G *Phys. Rev. B* **77** 155433 (2008)
41. Lozovik Yu E, Sokolik A A, Willander M *Phys. Status Solidi A* **206** 927 (2009)
42. Berman O L, Kezerashvili R Ya, Lozovik Yu E *Nanotechnology* **21** 134019 (2010)
43. Lozovik Y E, Sokolik A A *Pis'ma Zh. Eksp. Teor. Fiz.* **87** 61 (2008) [*JETP Lett.* **87** 55 (2008)]
44. Bistritzer R et al., arXiv:0810.0331
45. Kharitonov M Yu, Efetov K B *Semicond. Sci. Technol.* **25** 034004 (2010)
46. Lozovik Y E, Sokolik A A *Eur. Phys. J. B* **73** 195 (2010)
47. Lozovik Yu E, Sokolik A A *Phys. Lett. A* **374** 326 (2009)
48. Mink M P et al. *Phys. Rev. B* **84** 155409 (2011)
49. Lozovik Yu E, Ogarkov S L, Sokolik A A *Phys. Rev. B* **86** 045429 (2012)
50. Efimkin D K, Lozovik Yu E *Zh. Eksp. Teor. Fiz.* **140** 1009 (2011) [*JETP* **113** 880 (2011)]
51. Efimkin D K, Kulbachinskii V A, Lozovik Yu E *Pis'ma Zh. Eksp. Teor. Fiz.* **93** 238 (2011) [*JETP Lett.* **93** 219 (2011)]
52. Efimkin D K, Lozovik Yu E *Fullerenes, Nanotubes, Carbon Nanostruct.* **20** 569 (2012)
53. Keldysh L V, Kopaev Yu V *Fiz. Tverd. Tela* **6** 2791 (1964) [*Sov. Phys. Solid Sate* **6** 2219 (1965)]
54. Kozlov A N, Maksimov L A *Zh. Eksp. Teor. Fiz.* **48** 1184 (1965) [*Sov. Phys. JETP* **21** 790 (1965)]
55. Lozovik Yu E, Yudson V I *Pis'ma Zh. Eksp. Teor. Fiz.* **22** 556 (1975) [*JETP Lett.* **22** 274 (1975)]
56. Efimkin D K, Lozovik Yu E, Sokolik A A *Phys. Rev. B* **86** 115436 (2012); arXiv:1207.1817
57. Lozovik Yu E, Sokolik A A *Phys. Lett. A* **374** 2785 (2010)
58. Falkovsky L A *Usp. Fiz. Nauk* **178** 923 (2008) [*Phys. Usp.* **51** 887 (2008)]
59. Berman O L, Kezerashvili R Ya, Lozovik Yu E *Phys. Lett. A* **374** 3681 (2010)
60. Mikhailov S A, Ziegler K *Phys. Rev. Lett.* **99** 016803 (2007)
61. Koppens F H L, Chang D E, Javier García de Abajo F *Nano Lett.* **11** 3370 (2011)
62. Berman O L, Gumbs G, Lozovik Yu E *Phys. Rev. B* **78** 085401 (2008)
63. Kotov O V, Lozovik Yu E *Phys. Lett. A* **375** 2573 (2011)
64. Kotov O V, Lozovik Yu E *Fullerenes, Nanotubes, Carbon Nanostruct.* **20** 563 (2012)
65. Kotov O V, Lozovik Yu E, to be published
66. Berman O L, Kezerashvili R Ya, Lozovik Yu E *Phys. Rev. B* **82** 125307 (2010)
67. Apenko S M, Lozovik Yu E *Zh. Eksp. Teor. Fiz.* **89** 573 (1985) [*Sov. Phys. JETP* **62** 328 (1985)]
68. Efimkin D K, Lozovik Yu E, Sokolik A A *Nanoscale Res. Lett.* **7** 163 (2012)
69. Tse W-K et al. *Phys. Rev. Lett.* **105** 057401 (2010)
70. Efimkin D K, Lozovik Yu E, Sokolik A A *J. Magn. Magn. Mater.* **324** 3610 (2012); arXiv:1107.4695
71. Efimkin D K, Lozovik Yu E *Phys. Rev. B*, submitted; arXiv: 1208.3320
72. Raghu S et al. *Phys. Rev. Lett.* **104** 116401 (2010)
73. Lozovik Yu E, to be published

PACS numbers: 42.55.Ah, 42.70.Nq, 78.67.Bf
DOI: 10.3367/UFNe.0182.201210i.1116

Theory of the dipole nanolaser

I E Protsenko

1. Introduction

This paper is concerned with the theoretical investigation into the coherent generation of the dipole moment of a metallic nanoparticle, when a localized plasmon resonance is excited in it with the use of a generator (an atom, a quantum dot, etc.) in which an inverse electron state population is realized. The generator and the nanoparticle experience a near-field interaction. This nano-dimensional system — a 'dipole' nanolaser (DNL) — emits a coherent electromagnetic field when threshold conditions are fulfilled. We derive basic and simplified DNL equations, discuss the threshold lasing conditions and the DNL features associated with incoherent dipole moment generation, and take a look at several DNL-based facilities (broadband optical modulators, highly efficient light-emitting devices), as well as possible DNL designs and further lines of their theoretical investigation.

Research into the resonance interaction of electromagnetic radiation with metallic particles have a long-standing history [1–3]. Today, these studies are on the rise, and a new field of physics — nanoplasmonics [4] — has made its appearance, which is related to the development of nanotechnologies and the emergence of new practical tasks: to control light in optoelectronics [5, 6], enhance the efficiency of solar elements using metallic nanoparticles [7], etc. Metallic nanoparticles possessing localized plasmon resonances (LPRs) may be employed as antennas in the optical and near-infrared regions [8], including the production of nano-dimensional lasers. The method of coherent radiation generation and the dipole nanolaser based on this were proposed in patent [9]; the corresponding theory was elaborated in Refs [10–17] and applied, for instance, in Refs [18, 19]. Independently of and practically simultaneously with Ref. [9], the authors of patent [20] came up with a method of generating surface plasmons and a device for surface plasmon amplification by stimulated emission of radiation (spaser), which is close to the DNL. The theory of spacers was elaborated in Ref. [21] and in other work. Also investigated was the possibility of compensating losses in active media with metallic nanoparticles [22]; this loss compensation takes place both in DNLs and in spasers. Several experiments have been carried out with devices close to the DNL, which were operated both below [23, 24] and above [25, 26] the lasing threshold; the complete bibliography of DNL and spaser research is hard to expound on in this short report.

The aim of this paper is to briefly outline the theory of DNLs and to consider some of its new features. The DNL theory is based on the well-known equations of a single-mode laser [27], in which the electromagnetic field mode is replaced with the dipole moment arising from the resonance oscillations of the nanoparticle electron density. The quantum of linear electron density oscillations is a boson, like the quantum of an electromagnetic field (EMF), and coherent (laser) generation of electron density oscillations is therefore possible, similarly to coherent generation of EMF bosons. The feasibility of laser generation of not only EMF quanta, but also other bosons, for instance, Bose–Einstein condensates of atoms in traps [28], was emphasized earlier. Basic DNL equations substantiate the possibility of coherent generation not only of the dipole moment and radiation but of other laser effects in DNL-like systems as well. The elaboration of the basic equations results in progressively more realistic models of the DNL and its related devices. In doing so, it is possible to employ the well-known approaches of laser theory, for instance, in the description of spontaneous emission into a mode [29, 30], as well as of classical electrodynamics, for instance, in the description of DNL modes [3]. Those effects which are of little significance in 'classical' laser theory quite often turn out to be highly important for the DNL like, for instance, nonthreshold lasing [30] or local field effects [31]. Elaborating the basic DNL equations leads to models different from their analogs in laser theory; in particular, the equations for the DNL in an external field with the inclusion of spontaneous emission into a mode [17] are significantly different from the equations for an ordinary laser with external signal injection [27]. The DNL theory is highly instructive, because it combines, in a natural way, the classical effects of the nonlinear dynamics of oscillatory systems (threshold effects, bistability, etc.) and the special features of quantum electrodynamics (spontaneous emission, quantum noise, single-photon emission). This all makes the DNL an interesting subject of basic research, but its practical applications are equally interesting.

The paper outline is as follows. In Section 2, we offer the derivation of DNL equations, which is more general than in Ref. [10], without invoking the quasistatic approximation and the assumption that the nanoparticle dimensions are negligibly small. In Section 3, we simplify the basic equations: they are brought to the form of Ref. [10] convenient for applications; validity conditions of the equations are discussed and many-atom DNL equations are considered. Sections 4 and 5 are concerned with the DNL oscillation conditions and point to the possibility of bifurcations in lasing, when the direction of dipoles changes in a step-wise manner; also included is the incoherent (spontaneous) generation of the dipole moment of a few-atom DNL. In summary, we discuss the prospects of DNL theory development.

2. Basic equations of the dipole nanolaser

A simple DNL design comprises a metallic nanoparticle and a nearby emitting two-level system (atom, molecule, quantum dot, etc.) in which the population inversion of its states is effected with the aid of an incoherent external pump: a broadband light pulse, injection current, and so forth. (Fig. 1a). The localized plasmon resonance frequency ω_{LPR} of the metallic nanoparticle is close to the transition frequency ω_2 of the two-level system; the particles experience resonance interaction via EMF.

The equations for a two-level system [32] in an external resonance field $\mathcal{E} = \mathbf{e}[E(t)\exp(-\mathrm{i}\omega t) + E^{+}(t)\exp(\mathrm{i}\omega t)]$ are

I E Protsenko Lebedev Physical Institute,
Russian Academy of Sciences, Moscow, Russian Federation;
Plasmonics Ltd, Moscow, Russian Federation
E-mail: protsen@sci.lebedev.ru, protsenk@gmail.com

Uspekhi Fizicheskikh Nauk **182** (10) 1116 – 1122 (2012)
DOI: 10.3367/UFNr.0182.201210i.1116
Translated by E N Ragozin; edited by A Radzig

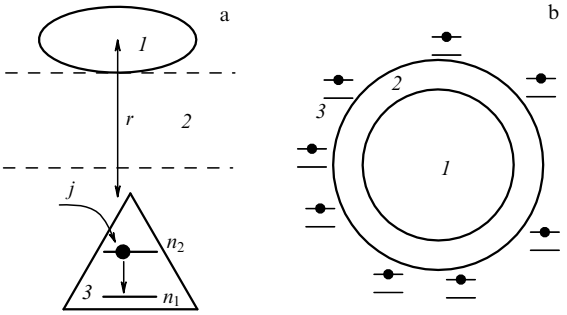

Figure 1. DNL diagrams: (a) metallic nanoparticle *1* is separated from the two-level system — quantum dot *3* — by a dielectric sublayer *2*; (b) 'core–shell' type DNL.

well known, where $\mathbf{e}$ is a unit vector, and the amplitude $E(t)$ varies more slowly than $\exp(-\mathrm{i}\omega t)$. In the approximation of slowly varying amplitudes, one has

$$\dot{D} = \frac{2\mathrm{i}\boldsymbol{\mu}\mathbf{e}}{\hbar}(E\sigma^+ - E^+\sigma) - \tau^{-1}(D - D_0)\,, \tag{1}$$

$$\dot{\sigma} = (\mathrm{i}\delta_2 - \Gamma_2)\sigma - \mathrm{i}\,\frac{\boldsymbol{\mu}\mathbf{e}}{\hbar}\,ED\,, \tag{2}$$

where D is the population inversion; $\boldsymbol{\mu}$ is the real dipole matrix element; τ^{-1} and Γ_2 are the relaxation rates of the population of the upper level in the two-level system and of its dipole moment, respectively; D_0 is the pump-induced equilibrium value of population inversion in the absence of the field, and $\delta_2 = \omega - \omega_2 \ll \omega_2$; the dipole moment of the two-level system $\hat{\mathbf{d}}_2 = \boldsymbol{\mu}[\sigma\exp(\mathrm{i}\omega t) + \sigma^+\exp(-\mathrm{i}\omega t)]$, and its magnetic moment is assumed to be zero; the resonance frequency of the transition between the states is $\omega_2 \approx \omega_{\mathrm{LPR}}$.

We replace σ in Eqn (2) by Bose operator a, $[a^+, a] = 1$, and at $D = -1$ arrive at the equation of motion for the dipole moment $\hat{\mathbf{d}}_0 = \boldsymbol{\mu}_0[a\exp(\mathrm{i}\omega t) + a^+\exp(-\mathrm{i}\omega t)]$ of the nanoparticle, i.e. the linear dipole (harmonic oscillator) in the resonance EMF:

$$\dot{a} = (\mathrm{i}\delta - \Gamma_{\mathrm{LPR}})a + \mathrm{i}\,\frac{\boldsymbol{\mu}_0\mathbf{e}}{\hbar}\,E\,, \tag{3}$$

where $\delta = \omega - \omega_{\mathrm{LPR}} \ll \omega_{\mathrm{LPR}}$, Γ_{LPR} is the LPR linewidth, and a may be termed the plasmon annihilation operator.

The two-level system is treated as a point dipole. The finite nanoparticle dimensions should be taken into consideration: the two-level system may be located closely to the nanoparticle, so that the field of the system changes markedly over the domain occupied by the nanoparticle. As a rule, the nanoparticle dimensions are smaller than the EMF wavelength, and the quasistatic approximation therefore applies inside the nanoparticle, and the polarization (the dipole moment of a unit volume) is the same throughout the nanoparticle [4]. Let us introduce the Bose operator $p(\mathbf{r})$ of polarization amplitude, $a = \int_V p(\mathbf{r})\,\mathrm{d}V$, where V is the nanoparticle volume. The commutation relations $[p(\mathbf{r}), p^+(\mathbf{r}')] = V\delta(\mathbf{r} - \mathbf{r}')$ ensure that $[a, a^+] = 1$ for the Bose operator a; $\mathbf{r}$ and $\mathbf{r}'$ are the radius vectors of the points inside the nanoparticle. The equation of motion for $p(\mathbf{r})$ has the form

$$\dot{p}(\mathbf{r}) = (\mathrm{i}\delta - \Gamma_{\mathrm{LPR}})\,p(\mathbf{r}) + \mathrm{i}\,\frac{\boldsymbol{\mu}_0\mathbf{e}}{V\hbar}\,E(\mathbf{r})\,.$$

By integrating both sides of this equation over the nanoparticle volume, we obtain

$$\begin{aligned} &\dot{a} = (\mathrm{i}\delta - \Gamma_{\mathrm{LPR}})a + \mathrm{i}\,\frac{\mu_0}{\hbar}\,\bar{E}_\mu\,, \\ &\bar{E}_\mu(r) = V^{-1}\int_V \mathbf{e}_\mu\mathbf{e}(\mathbf{r}')\,E(\mathbf{r}')\,\mathrm{d}^3r'\,, \end{aligned} \tag{4}$$

where $\bar{E}_\mu$ is the nanoparticle volume-averaged projection of the external field amplitude onto the polarization mode under excitation (in the present case, onto the direction of the nanoparticle's dipole moment), $\mathbf{e}_\mu$ is the unit vector aligned with the nanoparticle's dipole moment, and r is the nanoparticle center distance from the two-level system. For a spherical nanoparticle, $\bar{E}_\mu(r) = E(\mathbf{r})$ in the quasistatic approximation, which can be directly verified.

Now, it is possible to describe the interaction, via an alternating electric field, between the two-level system and the metallic nanoparticle, which are located in a uniform transparent medium with a refractive index n_2 and separated by some distance. The electric field induced by the particle in the seat of the two-level system will be denoted by the subscript 02, while the field produced by the two-level system in the seat of the nanoparticle will be denoted by the subscript 20. We use Eqns (1)–(3) to arrive at the system of equations of motion for both dipoles — the particle and the two-level system — with the inclusion of their dipole–dipole interaction:

$$\dot{D} = 2\mathrm{i}\,\frac{\boldsymbol{\mu}\mathbf{e}_{02}}{\hbar}(\sigma^+E_{02} - E_{02}^+\sigma) - \tau^{-1}(D - D_0)\,, \tag{5}$$

$$\dot{\sigma} = (\mathrm{i}\delta_2 - \Gamma_2)\sigma - \mathrm{i}\,\frac{\boldsymbol{\mu}\mathbf{e}_{02}}{\hbar}\,E_{02}D\,, \tag{6}$$

$$\dot{a} = (\mathrm{i}\delta - \Gamma_{\mathrm{LPR}})a + \mathrm{i}\,\frac{\langle\boldsymbol{\mu}_0\mathbf{e}_{20}E_{20}\rangle_V}{\hbar}\,, \tag{7}$$

where $\langle\ldots\rangle_V$ signifies averaging over the nanoparticle volume.

By using the expression for the Fourier component of the dipole radiation [33], the approximation of slowly varying amplitudes, and the spectral decomposition of $E_{02}(t)$ and $E_{20}(t)$ into Fourier integrals, it is possible to show that the electric field amplitudes entering into equations (5)–(7) are written down as

$$\begin{aligned} &\boldsymbol{\mu}\mathbf{e}_{02}E_{02}(t) = -\frac{\mu_0\mu}{r^3}\,\xi(k_2r)\sigma\left(t - \frac{n_2r}{c_0}\right), \\ &\boldsymbol{\mu}_0\mathbf{e}_{20}E_{20}(t) = -\frac{\mu_0\mu}{r^3}\,\xi^*(k_2r)a\left(t - \frac{n_2r}{c_0}\right), \\ &\xi(\rho) = \exp(\mathrm{i}\rho)\left[(1 - \rho^2 - \mathrm{i}\rho) + \cos^2\theta_{\mathrm{r}}(\rho^2 + 3\mathrm{i}\rho - 3)\right], \end{aligned} \tag{8}$$

where $\rho = k_2r$, r is the observation point distance from the dipole, $k_2 = n_2\omega/c_0$, $\mathbf{n}$ is a unit vector directed from the dipole to the point of observation, and θ_{r} is the angle between $\mathbf{n}$ and parallel vectors $\mathbf{d}_{0,2}$; this angle will be determined below. In the second of expressions (8), ξ^* appears, while ξ enters into the first one, because the fields from particle 0 to particle 2 and vice versa propagate in opposite directions. On the right sides of expressions (8) there are dipole polarization amplitudes delayed by a time n_2r/c_0 taken for the EMF to travel the interparticle distance.

Equations (5)–(8) constitute the DNL basic equations. Their variables are the population inversion D and the dipole moments σ and a. Electromagnetic fields do not enter into the

equations, and the fields outside of the DNL may be determined from expressions (8) and the corresponding expressions for the magnetic fields of the dipoles. In the DNL, the place of a field mode is occupied by nanoparticle polarization (dipole moment) mode a, which gave rise to the name 'dipole' nanolaser. Instead of the polarization of the nanoparticle, it is possible to consider the field inside it; in the quasistatic approximation and under the excitation of a 'dipole' mode, this field differs from the polarization only by a factor standing for the electric susceptibility of the nanoparticle material. In a similar way, it is possible to derive equations when another electron density oscillation mode, for instance, the quadrupole one with a different LPR frequency, rather than the dipole mode, is excited in the nanoparticle. The oscillation modes for the field (or polarization) inside and outside spherical particles are exactly known [3]: they may be applied to analyzing the DNL with large spherical particles, when the quasistatic approximation is invalid inside them. For small nonspherical nanoparticles, it is possible to use the quasistatic approximation when describing the particle polarizations (the fields inside the particles) and multipole expansions to describe the fields outside the particles [33].

Equations (5)–(8) are operator equations, and their variables are fluctuating quantities with intrinsic quantum fluctuations and those caused by dissipation. One way to solve such equations involves the employment of spectral decompositions and the addition of Langevin forces, as was done in Ref. [30]. To analyze the DLN, we replace below equations (5)–(8) with equations for the averages and 'uncouple' correlations (an analog of the moments method in statistical theory): higher-order moments, i.e., the averages of the products of fluctuating quantities, are replaced by lower-order moments — by the products of the averages.

3. Simplified equations, their validity conditions, and conditions for dipole nanolaser oscillation

Let us assume that the interparticle distance is short, so that the EMF delay time $\tau_r = n_2 r/c_0$ is short in comparison with the characteristic time of change of variables, and in Eqns (8) we can write

$$\sigma\left(t - \frac{n_2 r}{c_0}\right) \approx \sigma(t) - \tau_r \frac{d\sigma}{dt}, \qquad a\left(t - \frac{n_2 r}{c_0}\right) \approx a(t) - \tau_r \frac{da}{dt}. \tag{9}$$

For sufficiently short r, when $\tau_r\, d\sigma/dt \ll \sigma(t)$ and $\tau_r\, da/dt \ll a(t)$, the derivatives on the right-hand sides of expressions (9) can be neglected, and then the system of equations (5)–(7) assumes the form

$$\dot{D} = 2i(\Omega^*_{int} a^+ \sigma - \Omega_{int} \sigma^+ a) - \tau^{-1}(D - D_0), \tag{10}$$

$$\dot{\sigma} = (i\delta_2 - \Gamma_2)\sigma + i\Omega_{int} a D, \tag{11}$$

$$\dot{a} = (i\delta - \Gamma_{LPR})a - i\bar{\Omega}^*_{int}\sigma, \tag{12}$$

where the coupling constant

$$\Omega_{int} = \xi(k_2 r)\,\frac{\mu_0\,\mu}{\hbar r^3}, \qquad \bar{\Omega}^*_{int} = \frac{1}{V}\int_V \Omega^*_{int}\, dV, \tag{13}$$

$\Omega_{int} = \Omega_{int}(r)$, $\bar{\Omega}^*_{int} = \bar{\Omega}^*_{int}(r)$, and r is the two-level system distance from the nanoparticle center. For a spherical nanoparticle of radius a, in the quasistatic approximation, when $k_2 a < k_2 r \ll 1$, it turns out that $\bar{\Omega}^*_{int} = \Omega^*_{int}$. On the other hand, beyond the quasistatic approximation and for small particles, when $k_2 a \ll 1$ and $k_2 r \geqslant 1$, we may put $\bar{\Omega}_{int} = \Omega_{int}$, correct to at least $\sim a/r \ll 1$. Therefore, for small spherical nanoparticles if nothing else, it may be assumed that the condition $\bar{\Omega}_{int} = \Omega_{int}$ is always fulfilled with a high accuracy.

DNL equations (10)–(13) coincide with single-mode laser equations, for instance (on changing the notation) with Eqns (3.2) from Ref. [27]. This signifies that it is possible to directly take advantage of several results of laser theory in the DNL analysis, including the possibility of the coherent generation of a nanoparticle dipole moment by analogy with the coherent EMF mode generation in a conventional laser. As in the latter, the DNL may have a lasing threshold, although DNLs quite often turn out to be 'nonthreshold' (see below), unlike ordinary lasers which are nonthreshold only under special conditions [30].

Let us estimate when it is possible to neglect retardation in Eqns (8). The DNL operates (reaches a stationary mode, etc.) with a characteristic rate $\sim \Gamma_{LPR}$, i.e., $\dot{\sigma}/\sigma \sim \dot{a}/a \sim \Gamma_{LPR}$. The LPR quality factor $Q = \omega_{LPR}/(2\Gamma_{LPR})$. Considering these relations, we find the smallness condition for the delay time $\tau_r = n_2 r/c_0$:

$$\frac{n_2 r}{c_0}\,\Gamma_{LPR} = \frac{n_2 r}{c_0}\,\frac{\omega_{LPR}}{2Q} = \frac{k_2 r}{2Q} \ll 1 \text{ or } \quad r \ll r_{cr} = \frac{2Q}{k_2}. \tag{14}$$

Figure 2 depicts the dependence of Q on the radius a of a spherical gold nanoparticle in water, $n_2 = 1.33$. For the peak value of $Q = 33.8$ for $a = 19$ nm and $\lambda_{LPR} \equiv \omega_{LPR}/c_0 = 560$ nm, we obtain the validity condition for equations (10)–(12): $r \ll r_{cr} = 4.53$ μm. Therefore, when the atom is located at a distance of, say, 40 nm from the particle surface (although so long a distance is unnecessary), neglecting the small atomic dimensions we have $r = 0.06$ μm $\ll r_{cr} = 4.53$ μm. Even at $Q_{LPR} = 10$ — which is often the case in experiments — $r = 0.06 \ll r_{cr} = 1.34$, i.e., there is a safety margin of 1.5 orders of magnitude. This signifies that the retardation in Eqns (10)–(12) may be neglected.

Equations (10)–(12) can be generalized to describe DNLs of various designs: for instance, when there are $N > 1$ two-level systems (atoms) rather than one, each of the systems is located at a distance r_m from the nanoparticle center, as in Fig. 1b. Using the subscript m to mark the variables and parameters relating to the corresponding atom and introducing the variables $\bar{D} = N^{-1}\sum_{m=1}^{N} D_m$ and $\Sigma = N^{-1}\sum_{m=1}^{N} \Omega^*_m \sigma_m$ averaged over the atomic ensemble, where Ω_m is defined by expression (13) with $r = r_m$, one can

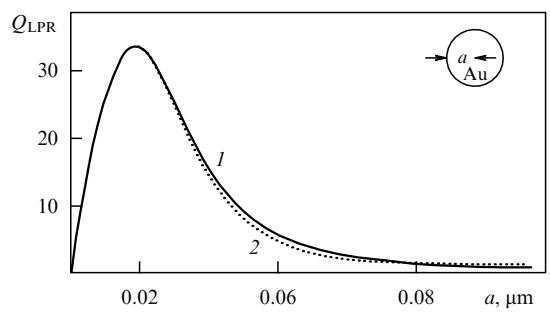

Figure 2. LPR quality factor as a function of the radius of a gold nanoparticle in water: *1* — result of an approximate solution to the dispersion equation [3], and *2* — exact solution of this equation.

obtain, in lieu of formulas (10)–(12), the following equations

$$\dot{\bar{D}} = 2\mathrm{i}(a^{+}\Sigma - \Sigma^{+}a) - \tau^{-1}(\bar{D} - D_0)\,, \tag{15}$$

$$\dot{\Sigma} = \left[\mathrm{i}(\delta_2 + \Omega_{dd}\bar{D}) - \Gamma_2\right]\Sigma + \mathrm{i}|\bar{\Omega}|^2 a\bar{D}\,, \tag{16}$$

$$\dot{a} = (\mathrm{i}\delta - \Gamma_{\mathrm{LPR}})a - \mathrm{i}N\Sigma\,. \tag{17}$$

The factor N in the last term on the right-hand side of Eqn (17) points to the contribution made by N atoms to the generation of a nanoparticle's dipole moment. A peculiar feature of Eqn (16) is the nonlinear resonance shift $\Omega_{dd}\bar{D}$, where the quantity Ω_{dd} describing 'local field' effects in the DNL, which are associated with atomic interactions via the EMF [31], is defined by expression (13) averaged over all atoms, with r being the interatomic distance. It may be shown that Ω_{dd} is a real quantity. The inclusion of Ω_{dd} fluctuations permits describing the effects of inhomogeneous broadening ('self-broadening') in many-atom DNLs.

4. Oscillation conditions for the dipole nanolaser

We revert to Eqns (10)–(12). Dipole matrix elements $\mu_{0,2}$ enter into expression (13) for the coupling constant, but polarizabilities, whose calculation is carried out at will for metallic nanoparticles, are more convenient to use than $\mu_{0,2}$. In Ref. [10], it was shown that $|\mu_0|^2 = \alpha_{0\mathrm{r}}\hbar\Gamma_{\mathrm{LPR}}$ and $|\mu_2|^2 = \alpha_{2\mathrm{r}}\hbar\Gamma_2$, where $\alpha_{0\mathrm{r}}$ and $\alpha_{2\mathrm{r}}$ are the respective resonance polarizabilities of the nanoparticle and the two-level system. Whence, and from expression (13), it is possible to obtain $|\Omega_{\mathrm{int}}|^2/(\Gamma_2\Gamma) = |\xi|^2|\alpha_{0\mathrm{r}}\alpha_{2\mathrm{r}}|/r^6$.

The nontrivial stationary solution of Eqns (10)–(12) is well known, in particular $D = D_{\mathrm{th}} \equiv (1+\delta^2/\Gamma_{\mathrm{LPR}}^2)\Gamma_2\Gamma_{\mathrm{LPR}}/|\Omega_{\mathrm{int}}|^2$. Apart from the nontrivial solution, there is a trivial stationary solution $a = \sigma = 0$, $D = D_0$. When the pump exceeds the threshold value, $D_0 > D_{\mathrm{th}}$, the trivial solution becomes unstable, and the nontrivial solution is realized, giving rise to the coherent generation of the dipole moment. Since the population of the upper state in the two-level system does not exceed unity, $D_{\mathrm{th}} < 1$ becomes the necessary condition for the generation, which is fulfilled for a sufficiently strong interaction between the particles. In the case of reaching exact resonance $\omega = \omega_2 = \omega_{\mathrm{LPR}}$, the necessary condition for DNL oscillation is given as follows

$$D_{\mathrm{th}}^{-1} = \frac{|\Omega_{\mathrm{int}}|^2}{\Gamma_2\Gamma_{\mathrm{LPR}}} > 1$$

or

$$|\xi|^2\,\frac{|\alpha_{0\mathrm{r}}\alpha_{2\mathrm{r}}|}{r^6} > 1\,, \tag{18}$$

i.e., the two-level system should be sufficiently close to the nanoparticle, so that their center distance r satisfies the inequality $r < r_{\mathrm{cr}} = |\xi|^{1/3}|\alpha_{0\mathrm{r}}\alpha_{2\mathrm{r}}|^{1/6}$.

The DNL threshold corresponds to the strongest interaction between the particles, i.e., according to inequality (18) to the maximum of the quantity $|\xi|^2/r^6$ in θ_{r} for a fixed r. An analysis made with the use of formulas (8) for a spherical nanoparticle suggests that the value of $|\xi|^2/r^6$ is greatest when $\cos\theta_{\mathrm{r}}$ equals 1 or 0, i.e., when the dipoles are directed parallel or perpendicular to the segment connecting them; this also follows from symmetry considerations. The maximum at $\cos\theta_{\mathrm{r}} = 1$ corresponds to $0 < k_2 r < \rho_{\mathrm{bif}}$, and in this case the near-field interaction of the dipoles prevails over their far-field interaction. The maximum at $\cos\theta_{\mathrm{r}} = 0$ corresponds to

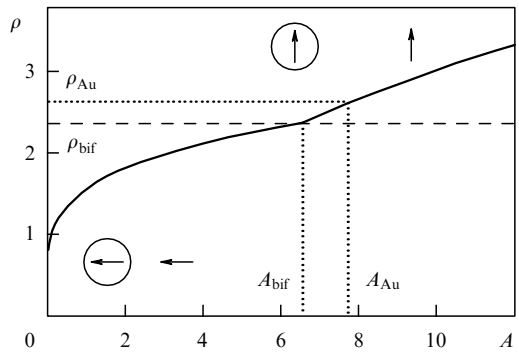

Figure 3. For a given value of A, the DNL oscillation is possible when $\rho < \rho_{\mathrm{cr}}(A)$, which is indicated with a solid curve. The curve break corresponds to ρ_{bif}; on exceeding it, the direction of the dipoles becomes perpendicular to their connecting straight line. The magnitude of A_{Au} and the critical value of ρ_{Au} correspond to a DNL made of a spherical gold nanoparticle and a quantum dot in silicon.

$k_2 r > \rho_{\mathrm{bif}}$ — the prevalent far-field interaction of the dipoles. At the point $k_2 r = \rho_{\mathrm{bif}} = (5+\sqrt{37})^{1/2}/\sqrt{2} \approx 2.35$, the dipole interaction energies at $\cos\theta_{\mathrm{r}} = 1$ and at $\cos\theta_{\mathrm{r}} = 0$ are equal and $|\xi(\rho_{\mathrm{bif}})|^2/\rho_{\mathrm{bif}}^6 \approx 0.154$. Therefore, as the value of $k_2 r$ changes, in going across $k_2 r = \rho_{\mathrm{bif}}$ bifurcation occurs: a stepwise change in the direction of dipole polarizations and the DNL radiation directivity. If advantage it taken of the variable $\rho = k_2 r$, the DNL oscillation condition (18) is conveniently written in dimensionless quantities:

$$A\,\frac{|\xi(\rho)|^2}{\rho^6} > 1\,,$$
$$\xi(\rho) = \begin{cases} 2\exp(\mathrm{i}\rho)(\mathrm{i}\rho - 1)\,, & 0 < \rho \leqslant \rho_{\mathrm{bif}}\,, \\ \exp(\mathrm{i}\rho)(1 - \rho^2 + \mathrm{i}\rho)\,, & \rho_{\mathrm{bif}} < \rho < \rho_{\mathrm{cr}} = k_2 r_{\mathrm{cr}}\,, \end{cases} \tag{19}$$

where $A = |\alpha_{0\mathrm{r}}\alpha_{2\mathrm{r}}|k_2^6$. Figure 3 depicts the dependence $\rho_{\mathrm{cr}}(A)$. The lasing is possible when $0 < \rho < \rho_{\mathrm{cr}}$. In this case, when $A > A_{\mathrm{bif}}$, two DNL oscillation modes are possible. The first is realized when $0 < \rho < \rho_{\mathrm{bif}}$ and the dipoles are parallel to the segment connecting them, and the second when $\rho_{\mathrm{bif}} < \rho < \rho_{\mathrm{cr}}$ and the dipoles are perpendicular to the segment connecting them. Accordingly, the far-field radiation patterns of the dipoles in these modes will be rotated relative to each other: this property may be employed for controling the DNL radiation. Several oscillation modes and the corresponding bifurcations may also exist for nonspherical nanoparticles. For $\rho_{\mathrm{bif}} < \rho < \rho_{\mathrm{cr}}$, the degeneracy shows up in directions of the dipoles in the plane perpendicular to the segment connecting the particle centers; in this case, the atom must be treated as a three-level system rather than a two-level one.

Let us estimate the value of A for a gold spherical particle 7 nm in radius. Let us assume that the two-level system (molecule) resides on a dielectric shell of a nanoparticle in water; the refractive index of the shell is little different from water's refractive index $n_2 = 1.33$; these conditions are close to the experimental ones accepted in Ref. [25]. We utilize the parameters of the two-level system as in Ref. [10] and the same parameters and formulas for calculating the dielectric function of gold and the polarizability of a gold nanoparticle as in Ref. [34]. In this case, $\lambda_{\mathrm{LPR}} = 525$ nm (in a vacuum), and $A = 6.28 \times 10^{-4}$, which corresponds to $\rho_{\mathrm{cr}} = 0.378$. The greatest center-to-center distance of the particles is $r_{\mathrm{cr}} = \rho_{\mathrm{cr}}\lambda_{\mathrm{LPR}}/(2\pi n_2) = 24$ nm. In Ref. [25], for $\lambda_{\mathrm{LPR}} = 520$ nm the

distance between a shell surrounding a gold spherical particle of radius 7 nm and the center of this particle was equal to 22 nm, i.e., our estimates bear out the possibility of lasing in Ref. [25].

By way of a second example, let us consider a DNL comprising a gold (or silver) spherical nanoparticle of radius 10 nm and a quantum dot in silicon. By using the dielectric function of silicon [35], we find that $\lambda_{\rm LPR} = 876$ (804) nm, $A = 7.8$ (6.7), and the dipoles may be spaced at a center-to-center distance $r < r_{\rm cr} = 100$ (83) nm. The corresponding points for the gold nanoparticle are indicated in Fig. 3; for this particle, $A = A_{\rm Au} > A_{\rm bif} \approx 7$, and the dipoles may therefore be directed along as well as across their connecting straight line. These estimates suggest that the necessary condition for DNL oscillation can be fulfilled in real systems.

5. Inclusion of incoherent dipole nanolaser oscillation

In this section we consider, following report [14], DNL equations in the next approximation of the moments method, including the averages of quadratic quantities, which will permit describing the incoherent dipole moment oscillation — an analog of incoherent oscillation, including the subthreshold one, in an ordinary laser [29]. Under incoherent oscillation conditions, the average values of the dipole moments $\langle\sigma\rangle = \langle a\rangle = 0$, but the corresponding energies, or the squares of the moduli of the dipole moments, are $\langle\sigma^+\sigma\rangle \neq 0$ and $\langle a^+a\rangle \neq 0$.

In equations (10)–(12) we go over from operators a and σ to their binary combinations: the operator of the number of plasmons, $n_0 = a^+a$, and $G = {\rm i}\Gamma_{\rm tot}^{-1}(\Omega_{\rm int}\sigma^+a - \Omega_{\rm int}^*a^+\sigma)$, where $\Gamma_{\rm tot} = \Gamma_{\rm LPR} + \Gamma_2$. In lieu of D it is more convenient to use the operator n_2 of the upper level population of the two-level system: $D = 2(n_2 - 1/2)$. We put $\delta_0, \delta \ll \Gamma_{\rm LPR}, \Gamma_2$ and consider the resonance case (which is more general than in Ref. [14]) and assume that there are N atoms equally spaced from a metal nanoparticle, for instance, on a dielectric shell (Fig. 1b). By differentiating the products of the operators and employing Eqns (10)–(12), we find that

$$\dot{G} = -2\Gamma_{\rm tot}G + 2g_{\rm pl}N\left[n_0\left(n_2 - \frac{1}{2}\right) + \frac{n_2}{2N}\right], \tag{20}$$

$$\dot{n}_0 = -2\Gamma_{\rm LPR}n_0 + \Gamma_{\rm tot}G, \tag{21}$$

$$\dot{n}_2 = -\Gamma_{\rm tot}G - \frac{n_2}{\tau} + j, \tag{22}$$

where j is the rate of pumping of an individual atom, $g_{\rm pl} = 2|\Omega_{\rm int}|^2/\Gamma_{\rm tot} \equiv 4\Gamma_2\Gamma_{\rm LPR}/(D_{\rm th}\Gamma_{\rm tot})$, n_0 is the number of plasmons per atom, and the total number of generated plasmons is Nn_0. In equations (20)–(22), the variables are the averages of the operators, and correlations are neglected, i.e., the averages are uncoupled: $\langle n_0n_2\rangle \approx \langle n_0\rangle\langle n_2\rangle$. In the derivation of equations (20)–(22), advantage was taken of the quantum-mechanical identity $\sigma^+\sigma = n_2$ [36], with the consequence that the term $n_2/(2N)$ responsible for the incoherent generation of a nanoparticle's dipole moment emerged in the square brackets on the right-hand side of Eqn (20). This term, which is proportional to n_2, makes a contribution to plasmon generation irrespective of the existence of population inversion: the greater N, the smaller is this term.

Figure 4 depicts the dependence of the number of plasmons generated by a DNL with $N = 100$ atoms on the pumping rate expressed in $\Gamma_{\rm LPR}$ units at $D_{\rm th} = 0.9$ and the same Γ_2 as in Ref. [10], i.e., $\Gamma_2 = \Gamma_{\rm 2R} + \Gamma_{\rm 2NR}$, where the radiative width of the line of the two-level system (a quantum dot) is $\Gamma_{\rm 2R} \equiv 1/\tau = 1$ ns, the nonradiative linewidth $\hbar\Gamma_{\rm 2NR} = \bar{e}\gamma_{\rm ac}T$, $\bar{e}$ is the electron charge, T is the temperature [K], $\gamma_{\rm ac} = 0.5 \times 10^{-6}$ eV K^{-1}; $T = 300$ K and $\Gamma_{\rm LPR} = 300\Gamma_{\rm 2R}$ (curve *1*), $\Gamma_{\rm LPR} = 10\Gamma_{\rm 2R}$ (curve *2*), and $\Gamma_{\rm LPR} = 3\Gamma_{\rm 2R}$ (curve *3*).

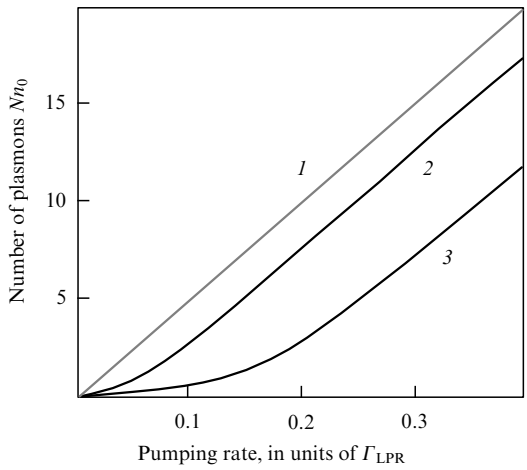

Figure 4. Number of plasmons generated by a DNL as a function of the pumping rate of each of $N = 100$ atoms, with the proviso that the population inversion be equal to 0.9 and the LPR linewidth be equal to 300 (curve *1*), 30 (curve *2*), and 3 (curve *3*) atomic radiation linewidths. The threshold character of oscillation is evident in curve *3*.

If the laser oscillation threshold is considered as a sharp acceleration of the growth in the number of plasmons upon increasing the pump current (the threshold in the number of plasmons), this threshold turns out to be evident only for curve *3*, when the LPR Q factor is quite high. Curves *1* and *2* correspond to 'nonthreshold' lasing. No less important than the existence or the absence of the threshold in the number of plasmons are the conditions for oscillation line narrowing to a value smaller than $\Gamma_{\rm LPR}$, which have not been investigated so far but may be found using the approach suggested in Ref. [30]. In view of the results of work [30], it may be assumed that inequality (18) remains the necessary condition for line narrowing even for 'nonthreshold' DNLs, which are described by curves like *1* and *2* in Fig. 4. It is significant that equations (20)–(22) predict a much higher pumping rate near the threshold: $j \sim \Gamma_{\rm LPR}$ instead of $j \sim 1/\tau \ll \Gamma_{\rm LPR}$ in the case of equations (10)–(12) disregarding the energy loss for incoherent subthreshold generation.

When $N \sim 1$, $\Gamma_{\rm LPR} \geqslant \Gamma_2$ (a low-Q LPR), $\Gamma_{\rm tot} \gg 1/\tau$, the number of plasmons $n_0 \ll 1$, and the pumping rate is not too high, $j \ll \Gamma_{\rm LPR}$, it is possible to neglect the term $\sim n_0$ in Eqn (20) and adiabatically eliminate G from Eqns (20)–(22) by putting $\dot{G} = 0$. After this, only a single equation remains: $\dot{n}_2 = -(\tau^{-1} + g_{\rm pl}/2)n_2 + j$. One can see from this equation that the electron lifetime in the upper state of the two-level system significantly shortens due to the presence of the metallic nanoparticle: under ordinary conditions $g_{\rm pl} \sim \Gamma_{\rm LPR} \gg \tau^{-1}$. This fact can be utilized for making broadband optical modulators with metallic nanoparticles [16].

In circumstances where $g_{\rm pl} \sim \Gamma_{\rm LPR} \gg \tau^{-1}$, upon adiabatic elimination of G it is possible to neglect the term n_2/τ in the equation for n_2. This signifies that the atom radiates primarily to the nanoparticle's 'dipole' mode and that the radiation to its other modes with frequencies different from the dipole mode frequency is negligible. Therefore, the number of

modes to which the atom may spontaneously radiate is limited, and in this sense the nanoparticle is similar to a photonic crystal. In this case, the stationary number of plasmons $n_0 = j/(2\Gamma_{\rm LPR})$ increases linearly with pump current, and there is no oscillation threshold in the number of plasmons, but the DNL linewidth may decrease to values smaller than $\Gamma_{\rm LPR}$, as with a nonthreshold laser [30]. It is noteworthy that, although there is absorption in the metallic nanoparticle, the number of photons delivered by the two-level system and reradiated by the particle is not so small in comparison with the number of photons emitted by the two-level system in the absence of the nanoparticle, the pump rate being the same in both cases. Indeed, metallic nanoparticle cross sections for absorption and scattering under the LPR conditions may be in the ratio of 1:2 [4], i.e., only every third photon delivered by the atom will participate in nanoparticle heating, while the remaining photons will go to its dipole radiation. In this case, the reradiation rate is approximately $\tau\Gamma_{\rm LPR}$ times (i.e., an order of magnitude or more) higher than the emission rate of the atom in the absence of the nanoparticle. Therefore, from the standpoint of converting the current of a high-power pump, the ensemble of atoms near the nanoparticle constitutes a highly efficient nano-dimensional light-emitting device.

6. Conclusions

The dipole nanolaser is a quantum electronic system remarkable for its basic properties and its possible practical applications. The uniqueness of the DNL lies, in particular, in the fact that it resides 'at the boundary' of the domain where quantum effects are significant, like spontaneous emission to an oscillation mode, as are classical nonlinear effects like the excitation of self-oscillations, etc. In the foregoing, it was impossible to consider all DNL-related quantum effects involving, for instance, superluminescence in DNL ensembles, oscillation line narrowing in overcoming the threshold, etc. Many classical nonlinear effects were not considered, either, like the DNL bistability in an external resonance field [14, 15]. Also of interest is to analyze a few-atom DNL — like a logic cell (a qubit) for a quantum computer, for instance, of the 'controlled NOT' type [37]. In the subthreshold generation, DNLs may be employed as efficient nanodimensional light emitters. To improve the efficiency of solar batteries and photodetectors, use can be made of a device 'inverse' to the DNL: when a nanoparticle — an optical antenna — receives a photon and transmits it via its near field to, for instance, a photocurrent-producing quantum dot. Extensive literature [7] is concerned with research aimed at improving the efficiency of solar elements with the help of metallic nanoparticles; the promise of quantum dot-based photoelectric converters, even without nanoantennas, is also recognized [38], but DNL photodetectors have not been considered so far. It is hard to foresee all promising DNL applications.

Different schemes of practical DNL realization are possible: notably, in the form of a metallic nanoparticle in a dielectric shell, on the surface of which the active atoms or molecules (for instance, dye molecules adsorbed from a solution with the nanoparticles) are located (Fig. 1b). This DNL scheme has been experimentally realized [25]. Calculations of this type of DNL can also be performed in the framework of the 'core–shell' nanoparticle model. The shells are treated as continuous media with corresponding (complex) refractive indices. Calculations for spherical nanoparticles can be performed using the well-known modes of a spherical cavity [3] without invoking the quasiclassical approximation. Also possible is the employment of a 'nanoparticle–two-level system' model, similar to the model presented above, with several radiating atoms (molecules). Another DNL scheme incorporates a nanoparticle antenna placed on the surface, say, of a semiconductor; located at a small (up to several dozen nanometers) depth below the surface is an active layer — a p–n junction, a quantum well, or a layer of quantum dots. There are examples of the practical implementation of such systems, and the enhancement of their electro- and photoluminescence due to metallic nanoparticles is well known [23, 24]. A theoretical description of this type of DNL must take into consideration the plane interfaces of the media and the electrodynamics of dipoles in stratified media [39]. Also conceivable are combinations of various DNL schemes, for instance, of metallic nanoparticles with active shells residing on semiconductor surfaces.

The DNL theory, relying on rather simple equations, is developing systematically, providing a way for describing complex DNL schemes, predicting new effects, and helping in the planning of experiments. This enables the researcher to make analytical estimates using the results of theoretical quantum electronics, plasmonics, and the theory of radiation–matter interactions. Next, by applying numerical techniques, it will be possible to carry out comprehensive simulations of experiments, as soon as they are planned in Russia.

References

1. Mie G *Ann. Physik* **330** 377 (1908)
2. Maxwell Garnett J C *Philos. Trans. R. Soc. London A* **203** 385 (1904)
3. Stratton J A *Electromagnetic Theory* (New York: McGraw-Hill, 1941) [Translated into Russian (Moscow – Leningrad: Gostekhizdat, 1948)]
4. Klimov V V *Nanoplazmonika* (Nanoplasmonics) (Moscow: Fizmatlit, 2009)
5. Orrit M *Nature Phys.* **3** 755 (2007)
6. Akimov A V et al. *Nature* **450** 402 (2007)
7. Catchpole K R, Polman A *Opt. Express* **16** 21793 (2008)
8. Mühlschlegel P et al. *Science* **308** 1607 (2005)
9. Zaimidoroga O A, Protsenko I E, Samoilov V N, Patent of the Russian Federation RU 2249278 C2 of 21.04.2003
10. Protsenko I E et al. *Phys. Rev. A* **73** 069902(E) (2006)
11. Protsenko I E, O'Reilly E P *Phys. Rev. A* **74** 033815 (2006)
12. Krotova K E, Protsenko I E, in *Nauchnaya Sessiya MIFI. Sb. Trudov* (Scientific Session of the MEPhI. Proceedings) Vol. 4 (Moscow: MIFI, 2007) p. 47
13. Krotova K E, Protsenko I E, in *Nauchnaya Sessiya MIFI. Sb. Trudov* (Scientific Session of the MEPhI. Proceedings) Vol. 2 (Moscow: MIFI, 2008) p. 61
14. Protsenko I E et al. *Proc. SPIE* **6889** 68890U (2008)
15. Protsenko I E et al. *J. Phys. Conf. Ser.* **107** 012010 (2008)
16. Protsenko I, Krotova K, in *Physics, Chemistry and Application of Nanostructures. Proc. of the Intern. Conf. on Nanomeeting 2009, Minsk, Belarus, 26 – 29 May 2009* (Eds V E Borisenko, S V Gaponenko, V S Gurin) (Singapore: World Scientific, 2009) p. 561
17. Krotova K E, Protsenko I E, in *Trudy Nauchnoi Sessii MIFI-2010* (Proc. Scientific Session MEPhI-2010) Vol. 4 (Moscow: NIYaU MIFI, 2010) p. 189
18. Andrianov E S et al. *Opt. Lett.* **36** 4302 (2011)
19. Lisyansky A A et al. *Phys. Rev. B* **84** 153409 (2011)
20. Stockman M, Bergman D, Patent US 2009236539 (A1) 2009-09-24 appl. on Jan 3, 2003
21. Bergman D J, Stockman M I *Phys. Rev. Lett.* **90** 027402 (2003)
22. Lawandy N M *Appl. Phys. Lett.* **85** 5040 (2004)
23. Pillai S et al. *Appl. Phys. Lett.* **88** 161102 (2006)

24. Biteen J S et al. *Appl. Phys. Lett.* **88** 131109 (2006)
25. Noginov M A et al. *Nature* **460** 1110 (2009)
26. Oulton R F et al. *Nature Lett.* **461** 629 (2009)
27. Khanin Ya I *Osnovy Dinamiki Lazerov* (Foundations of Laser Dynamics) (Moscow: Fizmatlit, 1999)
28. Oraevskii A N *Usp. Fiz. Nauk* **171** 681 (2001) [*Phys. Usp.* **44** 647 (2001)]
29. Siegman A E *Lasers* (Mill Valley, Calif.: Univ. Sci. Books, 1986)
30. Protsenko I E et al. *Phys. Rev. A* **59** 1667 (1999)
31. Girard C *Rep. Prog. Phys.* **68** 1883 (2005)
32. Allen L, Eberly J H *Optical Resonance and Two-Level Atoms* (New York: Wiley, 1975) [Translated into Russian (Moscow: Mir, 1978)]
33. Landau L D, Lifshitz E M *Teoriya Polya* (The Classical Theory of Fields) (Moscow: Nauka, 1988) [Translated into English (Oxford: Pergamon Press, 1980)]
34. Protsenko I E, Uskov A V *Usp. Fiz. Nauk* **182** 543 (2012) [*Phys. Usp.* **55** 508 (2012)]
35. Adachi S, Mori H, Ozaki S *Phys. Rev. B* **66** 153201 (2002)
36. Protsenko I E, Lugiato L A *Quantum Semiclass. Opt.* **8** 1067 (1996)
37. Protsenko I E et al. *Phys. Rev. A* **66** 062306 (2002)
38. Nozik A J *Physica E* **14** 115 (2002)
39. Tomaš M S *Phys. Rev. A* **51** 2545 (1995)

PACS numbers: 42.50.Nn, 73.20.Mf, 78.67.Pt, 81.05.Xj
DOI: 10.3367/UFNe.0182.201210j.1122

Quantum plasmonics of metamaterials: loss compensation using spasers

A P Vinogradov, E S Andrianov, A A Pukhov, A V Dorofeenko, A A Lisyansky

1. Introduction

Recent years have seen the development of a new field of optics — quantum plasmonics—which combines the advantages of plasmonics and quantum electronics [1–25]. Although plasmonics deals with wave phenomena, it operates on a scale much shorter than the light wavelength in a vacuum, which endows plasmonics with many features of near-field optics and creates a demand for plasmonics from modern nanotechnologies. In the first place, mention should be made of SERS (surface enhanced Raman scattering), the SPASER (surface plasmon amplification by stimulated emission of radiation), nanodimensional light sources [26–30], and numerous metamaterial-based devices [17, 31, 32]: energy concentrators and transmission lines on the order of several dozen nanometers in size, a superlens with a resolution exceeding the diffraction limit, cloakings, hyperlenses [33–40], etc. The small dimensions of these objects introduce quantum effects into their dynamics.

Since the principle of metamaterials operation is underlain by the plasmon resonance of metallic nanoparticles (NPs), artificial metamaterials exhibit rather high energy loss. The existence of losses in metamaterial-based devices gives rise to energy transfer inside of them, which is effected by near fields. The necessary and sufficient condition for the energy transfer by evanescent waves is the emergence of a phase difference among 'interfering' evanescent harmonics [41]. The emerging dephasing of harmonics, which form an ideal image, shows up in their destructive interference and breaking of the ideal image [42]. To compensate for the loss, the authors of Refs [43–51] proposed the employment of active (amplifying) media in artificial metamaterials. However, it follows from the foregoing that the ideal image is broken not only by energy dissipation, but also amplification in the medium. It is required that as precise as possible a loss compensation be achieved [43, 52, 53].

The utilization of active media in metamaterials leads inevitably to the formation of nanolasers inside of them. Among nanolasers, mention should be made of the dipole nanolaser [8, 10], the spaser [11, 54], and the magnetic-mode nanolaser [48, 49]. From the standpoint of loss compensation in metamaterials, spasers, whose experimental realization was reported in Ref. [55], have the greatest promise as a base element. Schematically, the spaser constitutes a quantum-plasmon device which consists of inversely excited two-level quantum dots (QDs) (a two-level tunneling system, TLS) surrounding plasmon NPs (the more realistic treatment of a four-level system does not introduce qualitatively new properties (see Refs [50, 56, 57])). The principle of spaser operation is similar to that of lasers: light amplification ensured by population inversion in combination with feedback, which is produced by the stimulated emission of a quantum system. To fulfill the conditions for stimulated emission by an inverted quantum system in the field of the wave previously radiated by this system, the quantum system is placed in a cavity, which localizes the generated mode. In a spaser, the role of photons is played by surface plasmons (SPs) of an NP. The localization of plasmons on the NP [11, 49, 54] furnishes the conditions for feedback realization. To state it in different terms, the generation and amplification of the NP's near-fields occur in spasers. The amplification of SPs proceeds due to radiationless energy transfer from QDs. The process relies on the dipole–dipole interaction (or any other near-field interaction [58]) between a QD and a plasmon NP. This mechanism can be treated as the principal one, because the probability of radiationless plasmon excitation is $(kr_{\mathrm{NP-TLS}})^{-3}$ times higher than the probability of radiative photon emission [15] ($r_{\mathrm{NP-TLS}}$ is the center-to-center distance of the NP and the QD, $k = 2\pi/\lambda$, where λ is the wavelength in a vacuum). Therefore, the efficient energy transfer from the QD to the NP is achieved due to the short distance between them, despite the fact that the plasmon resonance Q factor is rather low.[1] Due to the high efficiency of this process, an external optical wave which propagates through the metamaterial interacts with entire spasers rather than separately with the amplifying medium and separately with plasmon particles.

Like a laser, a spaser constitutes a self-oscillating system. Its dipole moment executes free-running oscillations whose frequency and amplitude are determined by the balance between pumping and dissipation. An external field can only synchronize the spaser operation, i.e., make the dipole moment oscillate at the frequency of the external field. The weak dependence of the amplitude of these oscillations on the

[1] Below, we neglect the emission of photons, and therefore the Purcell effect [59, 60] does not play an appreciable role and may be disregarded.

A P Vinogradov, E S Andrianov, A A Pukhov, A V Dorofeenko Institute for Theoretical and Applied Electromagnetics, Russian Academy of Sciences, Moscow, Russian Federation; E-mail: a-vinogr@yandex.ru
A A Lisyansky Department of Physics, Queens College of the City University of New York, USA

Uspekhi Fizicheskikh Nauk **182** (10) 1122 – 1130 (2012)
DOI: 10.3367/UFNr.0182.201210j.1122
Translated by E N Ragozin; edited by A Radzig

external field makes difficult the employment of spasers as nanodimensional devices, but these difficulties are not insurmountable. In particular, Stockman [12] came up with the idea that a spaser operating in the transient mode can be used as an amplifier. Therefore, spaser physics is interesting enough to be a research subject in its own right. Spaser physics constitutes a new area of optics — quantum plasmonics. For the development of metamaterial electrodynamics, however, of interest is the consideration of structures made up of ordered linear or two-dimensional spaser arrays rather than the treatment of a single spaser. In this case, collective interactions between spasers may significantly change the oscillation conditions and the properties of free-running spaser self-oscillations, and even give rise to new effects or instabilities in these structures. In this connection, along with plasmons localized on plasmon particles, of special interest are plasmons traveling along one-dimensional objects like wire, a chain of nanoparticles, or a groove in a metal [61–64]. The presence of an amplifying medium results in the amplification of one-dimensional plasmons [4, 23, 44, 65]. Although the presently existing theoretical estimates and experimental realizations in the area of quantum plasmonics rely on quite simple models, they show the promise of using spasers in the development of the elements of optical information facilities and optical computers.

In this report, we consider both individual and collective behavior of spasers in above-threshold oscillation.

2. Equations of spaser 'motion'

Since the SP wavelength $\lambda_{\rm SP}$ is much shorter than the radiation wavelength λ in a vacuum [15, 16], the spatial derivatives in the Maxwell equations are much greater than the temporal ones. Neglecting the latter permits describing the plasmon field in the quasistatic approximation [66, 67]. It turned out that this is also true when the spaser operates even in the radiating nanoantenna mode, i.e., when the Joule loss in a nanoparticle is lower than the radiative loss. Considering the modes of a small spherical NP of radius $r_{\rm NP} \ll \lambda$ shows the plasmon resonance frequency coincides with the frequency at which the NP is a half-wave antenna (resonator): a half of the plasmon wavelength fits into the sphere diameter [66].

Below, we shall consider the excitation of only the principal (dipole) SP mode with a frequency $\omega_{\rm SP}$. For a silver NP surrounded by silicon oxide (SiO_2), the permittivity values are well known [68]. Assuming that the NP radius $r_{\rm NP} \sim r \sim 10$ nm, we estimate the dipole moment of the NP near the plasmon resonance: $\mu_{\rm NP} \sim 200$ D. The dipole moment of a typical QD of size $r_{\rm TLS} \sim 10$ nm is $\mu_{\rm TLS} \approx 20$ D [69]. The NP–QD interaction adheres to a dipole–dipole one: $V = \hbar\Omega_{\rm R} \sim \mu_{\rm NP}\,\mu_{\rm TLS}/r^3$, and the constant of this interaction (the Rabi frequency $\Omega_{\rm R}$) turns out to be two orders of magnitude lower than the oscillation frequency [22]. This permits us to apply the slowly varying amplitudes approximation below.

At the plasmon resonance frequency, the NP polarization is described by the oscillator equation with eigenfrequency equal to the plasmon resonance frequency:

$$\ddot{\mathbf{d}}_{\rm NP} + \omega_{\rm SP}^2 \mathbf{d}_{\rm NP} = 0\,. \tag{1}$$

This oscillator is quantized in the standard way [59, 70]: the Bose operators are introduced in this case for the production $[\hat{\hat{a}}^{\dagger}(t)]$ and annihilation $[\hat{\hat{a}}(t)]$ of a dipole SP excited in the NP, which satisfy the commutation relation $[\hat{\hat{a}}(t), \hat{\hat{a}}^{\dagger}(t)] = 1$, and the Hamiltonian is expressed as

$$\hat{H}_{\rm SP} = \hbar\omega_{\rm SP}\,\hat{\hat{a}}^{\dagger}\hat{\hat{a}}\,. \tag{2}$$

In the case of a spherical NP, the electric dipole mode field is uniform inside the NP, $\mathbf{E}_1 = -\boldsymbol{\mu}_1/r_{\rm NP}^3$, and has the form $\mathbf{E}_1 = -\boldsymbol{\mu}_1/r^3 + 3(\boldsymbol{\mu}_1\mathbf{r})\mathbf{r}/r^3$ outside. The vector of a unit dipole moment $\boldsymbol{\mu}_1$ is a dimensional quantity, and henceforward we shall explicitly write the factor $|\boldsymbol{\mu}_1|$.

The energy $\hbar\omega_{\rm SP}$ of one plasmon is expressed as [71]

$$W_1 = \frac{1}{8\pi}\int_{V_{\rm NP}} \omega\,\frac{\partial\,{\rm Re}\,\varepsilon}{\partial\omega}\bigg|_{\omega_{\rm SP}} E_1 E_1^*\,{\rm d}V_{\rm NP} = \frac{|\boldsymbol{\mu}_1|^2}{6r_{\rm NP}^3}\,\omega\,\frac{\partial\,{\rm Re}\,\varepsilon}{\partial\omega}\bigg|_{\omega_{\rm SP}}\,, \tag{3}$$

where $V_{\rm NP}$ is the NP volume. Hence, the field produced by the NP can be written out as

$$\mathbf{E} = \sqrt{\frac{3\hbar r_{\rm NP}^3}{|\boldsymbol{\mu}_1|^2\,\partial\,{\rm Re}\,\varepsilon/\partial\omega}}\,\mathbf{E}_1(\mathbf{r})(\hat{\hat{a}} + \hat{\hat{a}}^{\dagger})\,,$$

and accordingly the dipole moment of the NP is $\hat{\mathbf{d}}_{\rm NP} = \boldsymbol{\mu}_{\rm NP}(\hat{\hat{a}} + \hat{\hat{a}}^{\dagger})$, where

$$\boldsymbol{\mu}_{\rm NP} = \sqrt{\frac{3\hbar r_{\rm NP}^3}{\partial\,{\rm Re}\,\varepsilon_{\rm NP}/\partial\omega}}\,\frac{\boldsymbol{\mu}_1}{|\boldsymbol{\mu}_1|^2}\,.$$

This is consistent [20, 21] with the 'classical' definition of the dipole moment [72]:

$$\mathbf{d}_{\rm NP} = \frac{\varepsilon_{\rm NP}(\omega) - \varepsilon_{\rm M}}{\varepsilon_{\rm NP}(\omega) + 2\varepsilon_{\rm M}}\,\mathbf{E}_1 r_{\rm NP}^3\,.$$

To describe the quantum dynamics of an NP and the two-level QD of a spaser, use can be made of a model Hamiltonian in the form [8, 54, 73]

$$\hat{H} = \hat{H}_{\rm SP} + \hat{H}_{\rm TLS} + \hat{V} + \hat{\Gamma}\,, \tag{4a}$$

where $\hat{H}_{\rm TLS}$ is the Hamiltonian of the two-level QD [16, 54, 74]:

$$\hat{H}_{\rm TLS} = \hbar\omega_{\rm TLS}\hat{\hat{\sigma}}^{\dagger}\hat{\hat{\sigma}}\,, \tag{4b}$$

operator $\hat{V} = -\hat{\mathbf{d}}_{\rm NP}\hat{\mathbf{E}}_{\rm TLS}$ defines the interaction between the two-level QD and the NP, and operator $\hat{\Gamma}$ describes the relaxation and pumping effects [74]. The operator of the QD dipole moment is $\hat{\mathbf{d}}_{\rm TLS} = \boldsymbol{\mu}_{\rm TLS}(\hat{\hat{\sigma}}(t) + \hat{\hat{\sigma}}^{\dagger}(t))$, where $\hat{\hat{\sigma}} = |g\rangle\langle e|$ is the transition operator between the excited $|e\rangle$ and ground $|g\rangle$ states of the QD, and $\boldsymbol{\mu}_{\rm TLS} = \langle e|\hat{\mathbf{d}}_{\rm TLS}|g\rangle$ is the transition dipole moment of the QD. Therefore, one obtains

$$\hat{V} = \hbar\Omega_{\rm R}(\hat{\hat{a}}^{\dagger} + \hat{\hat{a}})(\hat{\hat{\sigma}}^{\dagger} + \hat{\hat{\sigma}})\,,$$

where the Rabi frequency

$$\Omega_{\rm R} = \frac{\boldsymbol{\mu}_{\rm NP}\,\boldsymbol{\mu}_{\rm TLS} - 3(\boldsymbol{\mu}_{\rm TLS}\,\mathbf{e}_r)(\boldsymbol{\mu}_{\rm NP}\,\mathbf{e}_r)}{\hbar r^3}\,,$$

and $\mathbf{e}_r$ is a unit vector: $\mathbf{e}_r = \mathbf{r}/r$.

We assume that the QD transition frequency is close to the SP frequency, $\omega_{\rm SP} \approx \omega_{\rm TLS}$, and seek the solution in the form $\hat{\hat{a}}(t) \equiv \hat{a}(t)\exp(-{\rm i}\omega t)$ and $\hat{\hat{\sigma}}(t) \equiv \hat{\sigma}(t)\exp(-{\rm i}\omega t)$, where $\hat{a}(t)$ and $\hat{\sigma}(t)$ are slowly varying amplitudes. Then, neglecting rapidly oscillating terms $\sim \exp(\pm 2{\rm i}\omega t)$ (the rotating wave

approximation [74]), the interaction operator $\hat{V}$ can be written out in the form of the Jaynes–Cummings Hamiltonian [70]:

$$\hat{V} = \hbar\Omega_{\mathrm{R}}(\hat{a}^{\dagger}\hat{\sigma} + \hat{\sigma}^{\dagger}\hat{a})\,. \tag{4c}$$

We proceed from Hamiltonian (4) and employ the standard commutation relations $[\hat{a}, \hat{a}^{\dagger}] = \hat{1}$, $[\hat{\sigma}^{\dagger}, \hat{\sigma}] = \hat{D}$ for operators $\hat{a}(t)$, $\hat{\sigma}(t)$ and the population inversion operator $\hat{D}(t)$ to arrive at the following Heisenberg equations of motion [8, 75]:

$$\dot{\hat{D}} = 2\mathrm{i}\Omega_{\mathrm{R}}(\hat{a}^{\dagger}\hat{\sigma} - \hat{\sigma}^{\dagger}\hat{a}) - \frac{\hat{D} - \hat{D}_0}{\tau_D}\,, \tag{5}$$

$$\dot{\hat{\sigma}} = \left(\mathrm{i}\delta - \frac{1}{\tau_\sigma}\right)\hat{\sigma} + \mathrm{i}\Omega_{\mathrm{R}}\hat{a}\hat{D}\,, \tag{6}$$

$$\dot{\hat{a}} = \left(\mathrm{i}\varDelta - \frac{1}{\tau_a}\right)\hat{a} - \mathrm{i}\Omega_{\mathrm{R}}\hat{\sigma}\,, \tag{7}$$

where $\delta = \omega - \omega_{\mathrm{TLS}}$ and $\varDelta = \omega - \omega_{\mathrm{SP}}$ are frequency mismatches. The QD population inversion operator $\hat{D}(t) = \hat{n}_e(t) - \hat{n}_g(t)$, where $\hat{n}_e = |e\rangle\langle e|$ and $\hat{n}_g = |g\rangle\langle g|$ are the operators of the upper and lower QD level populations, with $\hat{n}_e + \hat{n}_g = 1$. It should be emphasized that the population inversion operator $\hat{D}(t)$ is 'slow' on the strength of its definition. The contribution of relaxation and pumping effects, which is denoted by operator $\hat{\Gamma}$ in Eqn (4a), is described in Eqns (5)–(7) by terms proportional to the relaxation rates τ_D^{-1}, τ_σ^{-1}, and τ_a^{-1}, and the operator $\hat{D}_0$ describes the population inversion produced by extraneous pumping in the QD [70, 74].

Strong dissipation in the NP makes this quantization scheme approximate and at the same time permits neglecting quantum correlations [8, 10]. This allows treating $\hat{D}(t)$, $\hat{\sigma}(t)$, and $\hat{a}(t)$ as complex quantities and replacing the Hermitian conjugation by the complex one [8, 10, 12, 43]. In this case, the quantity $D(t)$, which has the meaning of the difference between upper and lower level populations, will assume only real values, because the corresponding operator is Hermitian. The quantities $\sigma(t)$ and $a(t)$ have the meanings of dimensionless complex oscillation amplitudes of the dipole moments of the QD and the SP, respectively. Therefore, the spaser equations (5)–(7) in this approximation are single-mode optical Bloch equations [74].

3. Stationary spaser oscillation mode

Apart from the trivial solution $a = 0$, $\sigma = 0$, $D = D_0$ stable below the oscillation threshold, the system of equations (5)–(7) also has a nontrivial stationary solution:

$$a = \frac{\exp(\mathrm{i}\varphi)}{2}\sqrt{\frac{(D_0 - D_{\mathrm{th}})\tau_a}{\tau_D}}\,, \tag{8a}$$

$$\sigma = \frac{\exp(\mathrm{i}\psi)}{2}\sqrt{\frac{(D_0 - D_{\mathrm{th}})(\delta_{\mathrm{SP}}^2 + \tau_a^{-2})\tau_a}{\Omega_{\mathrm{R}}^2\tau_D}}\,, \tag{8b}$$

$$D = D_{\mathrm{th}}\,, \tag{8c}$$

which corresponds to stationary spaser oscillation with a frequency $\omega = (\omega_{\mathrm{SP}}\tau_a + \omega_{\mathrm{TLS}}\tau_\sigma)/(\tau_a + \tau_\sigma)$, and the phases φ and ψ satisfy the relation

$$\cos(\psi - \varphi) = \frac{1}{\sqrt{1 + \tau_a^2(\delta - \varDelta)^2}}\,.$$

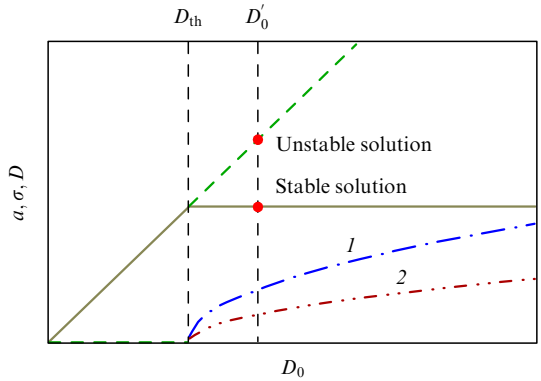

Figure 1. Stable stationary values of a (curve *1*), σ (curve *2*), and D (solid line) amplitudes. The unstable solution, which manifests itself for $D > D_{\mathrm{th}}$, is shown by a dashed line. The stable and unstable solutions at some pumping rate $D_0 = D_0'$ are marked with black circles.

This solution is stable when the pumping D_0 exceeds the threshold value

$$D_{\mathrm{th}} = \frac{1 + \varDelta^2\tau_a^2}{\Omega_{\mathrm{R}}^2\tau_a\tau_\sigma}\,. \tag{8d}$$

In this case, the stationary value of population inversion is fixed at the value of $D = D_{\mathrm{th}}$ and ceases to increase with enhancing pumping (Fig. 1) [8, 12, 43].

4. Transition to stationary oscillations, Rabi oscillations

The use of spaser-based metamaterials implies that this medium will modify the electromagnetic wave propagating through the medium. However, one would think that the existence of an eigenfrequency and an oscillation amplitude in a spaser is an impediment to the employment of spasers as inclusions which actively interact with the outer wave [6]. The interaction efficiency can be improved by operating in a transient mode. M Stockman's numerical experiments [12] suggest that a spaser exhibits complicated, strongly nonlinear dynamics during the transient regime. In this case, the spaser oscillation amplitude may be several times higher than the amplitude both of initial and of stationary spaser oscillations, i.e., the spaser can operate as an amplifier.

The transition of a spaser to stationary self-oscillations is defined by three characteristic times: the NP and QD polarization relaxation times τ_a and τ_σ, and the population inversion relaxation time τ_D. Due to high losses in metals, the time τ_a proves to be shortest. The experimental value is $\tau_a \sim (10^{-14} - 10^{-13})$ s [76], which coincides with the estimate obtained from classical electrodynamics [43]. Typical experimental values of remaining lifetimes are $\tau_\sigma = 10^{-11}$ s and $\tau_D = 10^{-13}$ s [77–79]. Therefore, for a metallic NP and a semiconductor QD, we obtain the following time scales: $\tau_a < \tau_D \ll \tau_\sigma$. The total self-oscillation settling time is defined by the longest time, $\sim \tau_\sigma$.

Numerical simulations have shown that the character of the transient process is heavily dependent on the initial value of the NP's dipole moment amplitude $a(0)$. For an initially 'cold' spaser, $a(0) \ll 1$, and the electric field of the NP is weaker than the field of the QD. In this case, the energy goes from the QD to the NP, and the $a(t)$ value tends to the stationary value (8a). For a high initial amplitude $a(0) \gg 1$, which may be achieved under the excitation of the NP by a nanosecond optical pulse [6, 12], the transient process is more complicated and proceeds two stages [22]. During the first

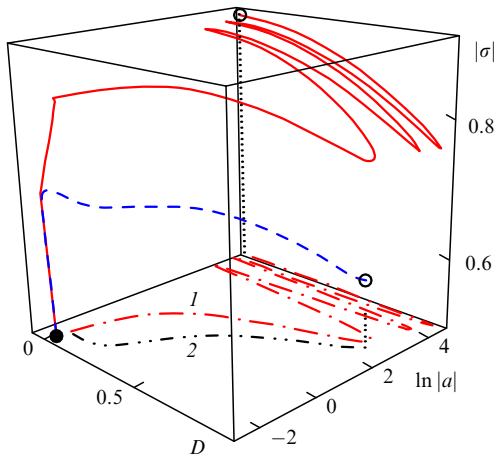

Figure 2. Spaser dynamics for $|\sigma| = 0.5$, $\tau_a = 10^{-14}$ s, $\tau_\sigma = 10^{-11}$ s, $\tau_D = 10^{-13}$ s, and $\Omega_R = 10^{13}$ s^{-1}. White dots correspond to the initial conditions for two trajectories emerging from $a(0) = 40 + 25\mathrm{i}$, $\sigma(0) = 0.9$, $D(0) = 0.05$ (solid line) and from $a(0) = 5$, $\sigma(0) = 0.65$, $D(0) = 0.9$ (dashed line). The stationary state is indicated with a black dot. Curves *1* and *2* correspond to the projections of these trajectories onto the plane $|\sigma| = 0.5$.

stage, the QD passes time in the strong NP field and the spaser self-oscillation amplitude experiences Rabi oscillations with a characteristic period $\tau_R = 2\pi/\Omega_R$. As this takes place, the energy flux periodically changes its direction from the NP to the QD and vice versa. Over a time of order $\tau_a \ln|a(0)|$, these oscillations decay due to dissipation in the NP and the QD. During the second stage, the spaser exhibits dynamics characteristic for small $a(0)$, when the spaser oscillation amplitude tends monotonically to the stationary value. For the time relation $\tau_a < \tau_D \ll \tau_\sigma$ typical for the spaser, its dynamics depend only slightly on τ_D. The total duration of the transient mode is on the order of τ_σ (Fig. 2).

The frequency of oscillations observed in numerical simulations can be easily estimated in the case of exact resonance $\delta = \Delta = 0$. By omitting the terms responsible for relaxation and pumping, which may be done at the initial stage of the process when all spaser variables are distant from their stationary values, we arrive at the reduced system of equations

$$\dot{a} = -\mathrm{i}\Omega_R \sigma\,, \tag{9}$$

$$\dot{\sigma} = \mathrm{i}\Omega_R a D\,, \tag{10}$$

$$\dot{D} = 2\mathrm{i}\Omega_R (a^*\sigma - \sigma^* a)\,. \tag{11}$$

Substitution of Eqn (9) and its conjugate into Eqn (11) gives the Newton equation

$$\frac{\mathrm{d}^2|a|}{\mathrm{d}t^2} = \frac{\partial U(|a|)}{\partial a} \tag{12}$$

for a 'particle' of unit mass with coordinate $|a|$, which moves in the potential $U(|a|) = 0.5(\Omega_R^2|a|^4 - C_1\Omega_R^2|a|^2)$, where C_1 is the integration constant [22]. The stable equilibrium position for this 'particle' is $|a|_{\mathrm{stable}} = \sqrt{C_1/2} = [\,|a(0)|^2 + D(0)/2]^{1/2}$, and the frequency of small oscillations about this equilibrium position is given by

$$\Omega = 2|a(0)|\Omega_R\,. \tag{13}$$

This expression coincides with the frequency of Rabi oscillations which emerge under the interaction of a two-level QD with a classical harmonic field of amplitude $a(0)$ or a quantized field with the number of photons approaching $\hat{a}^\dagger(0)\hat{a}(0) = n = |a(0)|^2$ [70].

5. Spaser in the field of an external optical wave, and spaser synchronization

Let us consider now the NP and QD dynamics in the field of an external optical wave $E(t) = E\cos(\nu t)$. Considering the external electric field as being classical and restricting ourselves to the dipole interaction, we write out the system's Hamiltonian in the form

$$\hat{H}_{\mathrm{eff}} = \hat{H} + \hbar\Omega_1(\hat{\tilde{a}}^\dagger + \hat{\tilde{a}})\left[\exp(\mathrm{i}\nu t) + \exp(-\mathrm{i}\nu t)\right] + \hbar\Omega_2(\hat{\tilde{\sigma}}^\dagger + \hat{\tilde{\sigma}})\left[\exp(\mathrm{i}\nu t) + \exp(-\mathrm{i}\nu t)\right]\,, \tag{14}$$

where $\hat{H}$ is defined by expression (4), and $\Omega_1 = -\boldsymbol{\mu}_{\mathrm{NP}}\mathbf{E}/\hbar$ and $\Omega_2 = -\boldsymbol{\mu}_{\mathrm{TLS}}\mathbf{E}/\hbar$ are the coupling constants of the NP and the QD to the external field.

As before, the equations of motion are the Heisenberg equations for the slowly varying amplitudes of operators $\hat{a}$, $\hat{\sigma}$, and $\hat{D}$:

$$\dot{\hat{D}} = 2\mathrm{i}\Omega_R(\hat{a}^\dagger\hat{\sigma} - \hat{\sigma}^\dagger\hat{a}) + 2\mathrm{i}\Omega_2(\hat{\sigma} - \hat{\sigma}^\dagger) - \frac{\hat{D} - \hat{D}_0}{\tau_D}\,, \tag{15}$$

$$\dot{\hat{\sigma}} = \left(\mathrm{i}\delta_E - \frac{1}{\tau_\sigma}\right)\hat{\sigma} + \mathrm{i}\Omega_R\hat{a}\hat{D} + \mathrm{i}\Omega_2\hat{D}\,, \tag{16}$$

$$\dot{\hat{a}} = \left(\mathrm{i}\Delta_E - \frac{1}{\tau_a}\right)\hat{a} - \mathrm{i}\Omega_R\hat{\sigma} - \mathrm{i}\Omega_1\,. \tag{17}$$

Here, $\delta_E = \nu - \omega_{\mathrm{TLS}}$ and $\Delta_E = \nu - \omega_{\mathrm{SP}}$ are frequency mismatches in the external optical field.

System of equations (15)–(17) has three stationary solutions $\{a_i, \sigma_i, D_i\}$, $i = 1, 2, 3$. A linear stability analysis of these solutions: $a(t) - a_i \sim \exp(\lambda t)$, $\sigma(t) - \sigma_i \sim \exp(\lambda t)$, and $D(t) - D_i \sim \exp(\lambda t)$ showed that only the solutions located in the lower branch of the curves depicted in Figs 3a and 3b are stable ($\mathrm{Re}\,\lambda < 0$). For a zero mismatch $\Delta_E = \delta_E = 0$ in the absence of the field, the points indicated in Fig. 3a correspond to the points indicated in Fig. 1. For a nonzero mismatch, the stable solution branch $D(E)$ exists only when the field amplitude is sufficiently large: $E > E_{\mathrm{synch}}(\Delta_E)$ (Fig. 3b).

Therefore, the value $E_{\mathrm{synch}}(\Delta_E)$ is the lower boundary of the domain in which the spaser can by locked by an external wave. Such threshold behavior is typical for nonlinear systems experiencing external action, and the range of parameters E and Δ_E in which locking occurs is termed the Arnold tongue [80–82]. The boundary of the Arnold tongue can be qualitatively obtained by treating the external wave as a perturbation.

In the zero approximation in the field amplitude E, system (15)–(17) has the stationary solution (5)–(7). Let us find the solution in the first approximation in the field amplitude E. By substituting $a = |a|\exp(\mathrm{i}\varphi)$ and $\sigma = |\sigma|\exp(\mathrm{i}\psi)$ into Eqn (17), we obtain

$$\frac{\mathrm{d}|a|}{\mathrm{d}t}\exp(\mathrm{i}\varphi) + \mathrm{i}\,\frac{\mathrm{d}\varphi}{\mathrm{d}t}\,|a|\exp(\mathrm{i}\varphi) = \left(\mathrm{i}\Delta_E - \frac{1}{\tau_a}\right)|a|\exp(\mathrm{i}\varphi) - \mathrm{i}\Omega_R|\sigma|\exp(\mathrm{i}\psi) - \mathrm{i}\Omega_1\,. \tag{18}$$

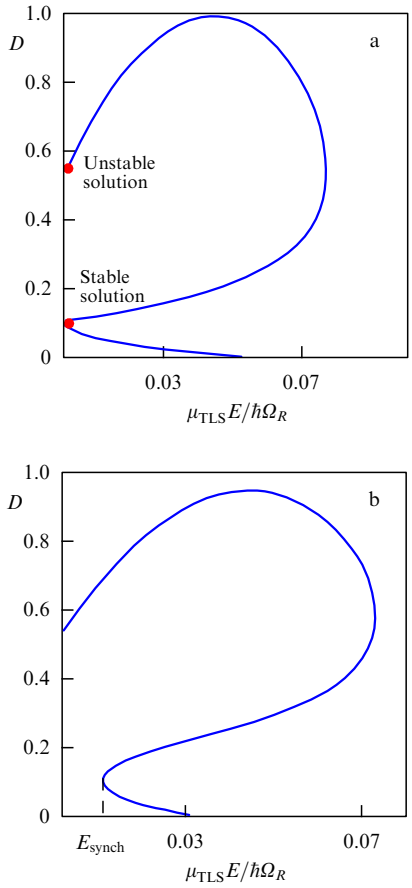

Figure 3. Stationary value of the population inversion D as a function of the external field amplitude for $\tau_a = 10^{-14}$ s, $\tau_\sigma = 10^{-11}$ s, $\tau_D = 0.5 \times 10^{-14}$ s, and $\Omega_{\rm R} = 10^{13}$ s^{-1}: (a) $\Delta_E = \delta_E = 0$, and (b) $\Delta_E = \delta_E = 10^{11}$ s^{-1}.

We divide both sides of Eqn (18) by $|a| \exp(\mathrm{i}\varphi)$ to bring the imaginary part of the equation to the form

$$\dot{\varphi} = \Delta_E - \Omega_{\rm R} \frac{|\sigma|}{|a|} \cos(\psi - \varphi) - \frac{\Omega_1}{|a|} \cos\varphi\,. \tag{19}$$

Substituting the quantities (8) into Eqn (19) in place of $|a|$, $|\sigma|$, and $\cos(\psi - \varphi)$ yields the equations of motion [8, 22] of an overdamped 'particle' with a coordinate φ:

$$\dot{\varphi} = -\frac{\partial \Phi(\varphi)}{\partial \varphi} \tag{20}$$

in the potential $\Phi(\varphi) = -\Delta_E \varphi + \Omega_1 \sin\varphi/|a|$.

The phase dynamics are the sliding of this 'particle' over the potential profile in a viscous liquid. For $|\Omega_1| < |a\Delta_E|$, there occurs a unidirectional motion. The particle velocity oscillates with the period tending to infinity as the critical situation $|\Omega_1| = |a\Delta_E|$ is approached. For $|\Omega_1| > |a\Delta_E|$, the particle finds itself in one of the minima of the potential function $\Phi(\varphi)$, which corresponds to the synchronization mode: the oscillation phase φ is 'locked' and ceases to vary in time. Therefore, the spaser's Arnold tongue is wedge-shaped in the low-field domain $E \ll \hbar\Omega_{\rm R}/\mu_{\rm NP}$.

Numerical simulations have shown that the boundary of the locking domain is described by the curve $E_{\rm synch}(\Delta_E)$ (Fig. 4). Outside of this domain, the solution irregular in time, which corresponds to chaotic spaser behavior.

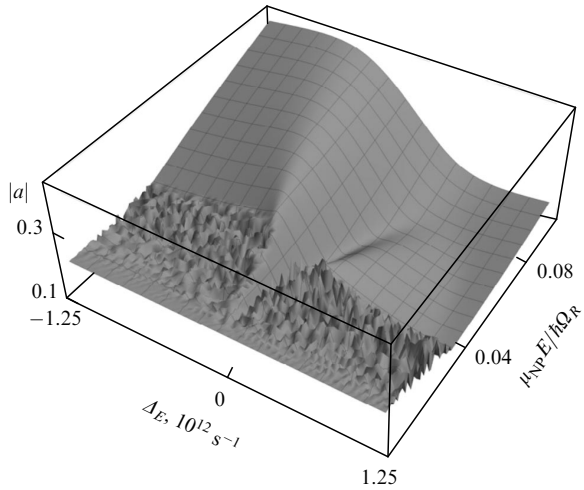

Figure 4. Dimensionless NP dipole moment as a function of external optical field amplitude E and frequency mismatch Δ_E. The speckle structure for small amplitudes of the external field corresponds to chaotic behavior of the dipole moment.

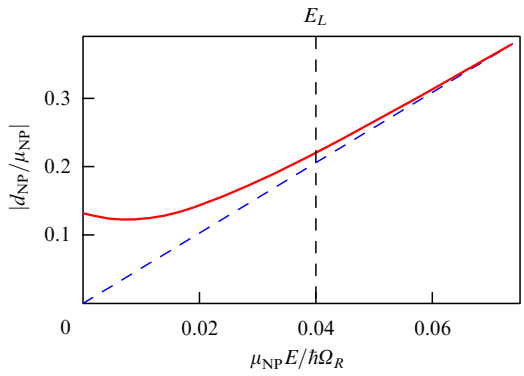

Figure 5. Amplitude of the NP dipole moment as a function of the magnitude of the external field for a zero mismatch.

Notice that a spaser which has reached the stationary state responds to the long-term ($\gg \tau_\sigma$) action of an external field in a qualitatively different manner than does a spaser exposed to a 'pulsed' ($\ll \tau_D$) external field, when the change in population inversion caused by the external field may be disregarded. While in the former case the response is nonlinear, in particular in a weak field $E \sim E_{\rm synch}(\Delta_E)$ the dipole moment does not depend on the external field at all and is defined by the frequency mismatch and the pumping level (Fig. 5), in the latter case the spaser's dipole moment is proportional to the external field [50, 56, 57].

In the absence of pumping ($D_0 = -1$), the solution of optical Bloch equations yields the answer close to the predictions of the classical theory describing the response of a single NP: the real part of an NP's dipole moment can assume both positive and negative values, depending on the frequency, but its imaginary part is always positive. This corresponds to the energy transfer from the external field to the spaser. In the presence of a pump close in frequency to the spaser oscillation frequency, the imaginary part of the dipole moment may assume negative values for certain values of Δ_E, which corresponds to the energy transfer from the spaser to the external field (Fig. 6) [20].

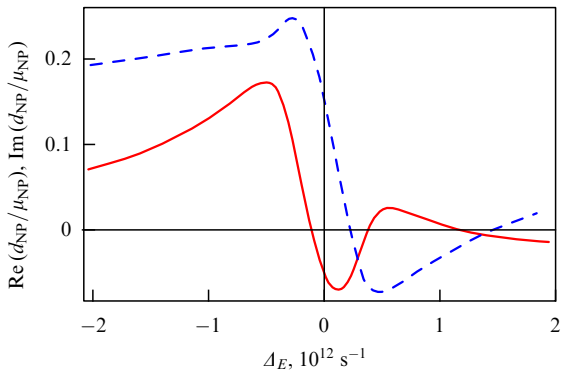

Figure 6. Real (solid curve) and imaginary (dashed curve) parts of the NP dipole moment as functions of frequency mismatch Δ_E for an external field amplitude exceeding the locking threshold, $E > E_{\text{synch}}(\Delta_E)$.

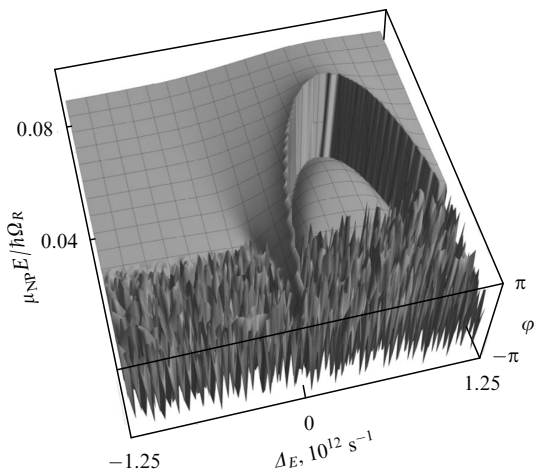

Figure 7. Dependence of $\varphi = \tan^{-1}(\text{Im}\, d_{\text{NP}}/\text{Re}\, d_{\text{NP}})$ on external field amplitude E and mismatch Δ_E. The smooth part of the surface corresponds to the Arnold tongue region in which the spaser is synchronized by the external field. In the discontinuity line $E_{\text{com}}(\Delta_E)$, where $\varphi = \pi$, the energy losses are precisely compensated.

It should be emphasized that for a given magnitude of external field there are two frequencies at which the imaginary part of the dipole moment turns to zero, i.e., complete compensation occurs (see Fig. 6). These points lie on the complete compensation curve $E = E_{\text{com}}(\Delta_E)$ (Fig. 7), which is defined by the expression [20]

$$\left(\frac{\mu_{\text{NP}} E_{\text{com}}(\Delta_E)}{\hbar}\right)^2 = \frac{1}{4}\left[-\frac{\tau_D \tau_\sigma^3}{\tau_a}\Delta_E^4 + D_0 \Omega_{\text{R}} \tau_\sigma^3 \frac{\mu_{\text{TLS}}}{\mu_{\text{NP}}}\frac{\Delta_E^3}{\tau_D} - \left(\frac{\tau_\sigma}{\tau_D} - \Omega_{\text{R}}^2 D_0 \frac{\tau_a \tau_\sigma^2}{\tau_D}\right)\Delta_E^2\right]\left(\tau_\sigma \Delta_E \frac{\mu_{\text{TLS}}}{\mu_{\text{NP}}} + \tau_a \Omega_{\text{R}}\right)^{-2}. \tag{21}$$

As $\Delta_E \to 0$, expression (21) changes into

$$\left(\frac{\mu_{\text{NP}} E}{\hbar}\right)^2 = (D_0 - D_{\text{th}})\Delta_E^2 \left(\frac{\tau_\sigma^2}{\tau_D \tau_a}\right).$$

Therefore, $E \propto (D_0 - D_{\text{th}})^{1/2}\Delta_E$, and this curve lies inside of the Arnold tongue [20].

Figure 7 depicts the phase difference between the NP dipole moment and the external field, which was obtained by the numerical solution of system (15)–(17). The discontinuity line, or the compensation line $E_{\text{com}}(\Delta_E)$, corresponds to a phase difference π, when the imaginary part of the dipole moment is equal to zero. In this case, the real part of the NP dipole moment turns out to be negative.

If the external field amplitude corresponds to a point lying below the compensation curve, the energy is transferred from the spaser to the field, and as the wave field propagates over the system of spasers, its amplitude should increase, approaching the value $E_{\text{com}}(\Delta_E)$. When the point lies above the curve, the energy will be absorbed inside the spaser, and the wave will attenuate and tend to the same value of amplitude. It is therefore expected that a wave will propagate over the system, whose amplitude will stably tend to the value defined by the level of spaser pumping and the frequency mismatch.[2]

The above reasoning relies on our analysis of the behavior of a single spaser. Moving from a single spaser to a spaser system may give rise to collective effects due to interspaser interaction, which may qualitatively change the picture of wave propagation through the active metamaterial.

6. Collective excitations of a spaser chain

So, we have ascertained that a spaser may synchronize its operation under the action of an external field. However, to make metamaterials requires the knowledge of how a spaser system works. In this case, collective interspaser interaction may significantly change the operating conditions and result in new effects. Indeed, since the times of Huygens it has been known that self-oscillating systems may synchronize their operation in the presence of even a weak interaction between them [81, 82]. Similar phenomena may also take place in a spaser system.

Below, we consider the collective interaction of spaser self-oscillations in the course of lasing above threshold by the simplest example of a linear spaser array. Two scenarios of the operation of the spaser system are possible in this case. First, the operation of all spasers may be synchronized, resulting in their in-phase operation. Second, a scenario is possible whereby the QD excitation will be transferred to their collective mode [2, 23, 65, 83, 84]. The role of collective mode is played by the dipole moment wave traveling along the chain of plasmon nanoparticles (see Ref. [60] and references cited therein).

For small frequency departures from the plasmon frequency, the dispersion relation for the wave of dipole moments traveling over an NP chain assumes the form

$$\omega(k) = \omega_{\text{SP}} + \gamma_i \frac{\omega_1^2}{\omega_{\text{SP}}}\cos(kb), \tag{22}$$

where $\omega_1^2 = r_{\text{NP}}^3 \omega_{\text{pl}}^2/(3b^3)$, $\gamma_1 = 1$ for longitudinal modes, and $\gamma_1 = -2$ for transverse ones [60]. This solution becomes meaningless for $k < k_0 = \omega/c$, when the mode turns into a leaky one (see Ref. [85]), i.e., the radiation of photons occurs. For a single spaser, the radiationless excitation of plasmons prevails over the emission of photons for $(k_0 r_{\text{NP-TLS}})^3 \ll 1$, where $r_{\text{NP-TLS}}$ defines the characteristic scale of the system. In

[2] We emphasize: if a weak wave propagating over the system of spasers in the stochastic regime (outside of the Arnold tongue) were amplified, the system would be unstable. It would then be possible to observe spontaneous excitation of a wave with its amplitude defined by the 'compensation line'.

the case of the collective mode, for a scale length r we must take k^{-1}, i.e., for $k < k_0$ we obtain $(k_0 r)^3 \geqslant 1$, and the energy will be transferred primarily to photons. Owing to the mutual synchronization of the spasers ($k = 0$), an effect similar to that considered in Ref. [14], where all spasers radiate in the same direction, should be observable in this situation.

The dipole–dipole interaction between the neighboring spasers gives rise to additional terms in Hamiltonian (4). Along with Ω_{R}, $\Omega_{\mathrm{NP-NP}}$ — the coupling constant between nearest-neighbor NPs, $\Omega_{\mathrm{NP-TLS}}$ — the coupling constant between the QD and the neighboring NPs, and $\Omega_{\mathrm{TLS-TLS}}$ — the coupling constant between the nearest-neighbor QDs, appear.

The inclusion of $\Omega_{\mathrm{NP-NP}}$ alone leads to the solution in the form of a harmonic wave with the dispersion equation

$$\omega_k = \omega_a + \Omega^{\mathrm{eff}}_{\mathrm{NP-NP}} \cos(kb)\,,$$

where $\Omega^{\mathrm{eff}}_{\mathrm{NP-NP}} = 2\Omega_{\mathrm{NP-NP}}\tau_a/(\tau_a + \tau_\sigma)$. This solution exists provided that the pumping exceeds the threshold value equal to

$$D_{\mathrm{th}}(k) = \frac{1 + (\Omega^{\mathrm{eff}}_{\mathrm{NP-NP}}\tau_\sigma)^2 \cos^2(kb)}{\Omega_{\mathrm{R}}^2 \tau_a \tau_\sigma}\,.$$

Despite the superficial similarity between the dispersion equations for the waves propagating over an NP chain and a spaser chain, there is a fundamental difference between these systems. First, the amplitude of waves propagating over the spaser chain is fixed and determined by the pumping level:

$$a_{n,k} = \frac{1}{2}\exp(\mathrm{i}\varphi)\sqrt{\left[D_0 - \frac{1 + (\Omega^{\mathrm{eff}}_{\mathrm{NP-NP}}\tau_\sigma)^2 \cos^2(kb)}{\Omega_{\mathrm{R}}^2 \tau_a \tau_\sigma}\right]\frac{\tau_a}{\tau_\sigma}}\,. \tag{23}$$

This autowave is different from solutions like solitons and kinks, which are known for other nonlinear systems [86], being a purely harmonic wave. Second, while the linear array of NPs obeys the superposition principle, an unusual situation takes place in the case of the chain of spasers: all autowaves, with the exception of the one with $k = \pm\pi/2b$, are unstable, and any initial perturbation evolves into this wave.

The inclusion of QD interaction with the neighboring NPs changes the situation qualitatively. The threshold pumping level becomes

$$D_{\mathrm{th}}(k) = \frac{1 + (\tau_\sigma \Omega^{\mathrm{eff}}_{\mathrm{NP-NP}})^2 \cos^2(kb)}{\left[\Omega_{\mathrm{R}} + 2\Omega_{\mathrm{NP-TLS}}\cos(kb)\right]^2 \tau_a \tau_\sigma}\,,$$

and the stability condition coincides with the condition for the minimum of $D_{\mathrm{th}}(k)$ (Fig. 8).

One can see from Fig. 8 that a critical value exists for the coupling constant

$$\Omega^*_{\mathrm{NP-TLS}} = \frac{1}{2}(\tau_\sigma \Omega^{\mathrm{eff}}_{\mathrm{NP-NP}})^2 \Omega_{\mathrm{R}}$$

which separates frequency-dispersive waves from waves with $k = \pm\pi/b$ or $k = 0$ (Fig. 9). Waves with $k < k_0$ cannot travel along the linear chain, because they become leaky waves in this case [85].

7. Conclusion

There is a great demand for devices capable of manipulating light in domains smaller than the optical wavelength, i.e., measuring about ten nanometers: SNOM (scanning near-field microscopy), SERS, optoelectronic devices, etc. It is evident that coherent nanodimensional sources of optical radiation, i.e., nanolasers, rank with these devices. Among the possible ways of their realization is the spaser, with a plasmon nanoparticle fulfilling the function of a laser cavity.

However, it turns out that a spaser can be employed not only as a separate, ultrafast (with a response time of several femtoseconds) device, but also as an active inclusion in nanocomposites, including metamaterials. Indeed, a spaser-based composite material constitutes a new nonlinear object of research with unique properties. The spaser experiences Rabi oscillations in the transition to a stationary spasing mode, and therefore the properties of this material can be controlled by the intensity of external optical perturbation. In the stationary mode, the material reacts to the perturbation frequency by going from stochastic oscillations to the propagation of plasmon autowaves; the amplitude of the propagating waves depends only slightly on the amplitude of the incoming signal and is controlled primarily by the pumping level. These materials may show promise and find application in optoelectronics and metaplasmonics.

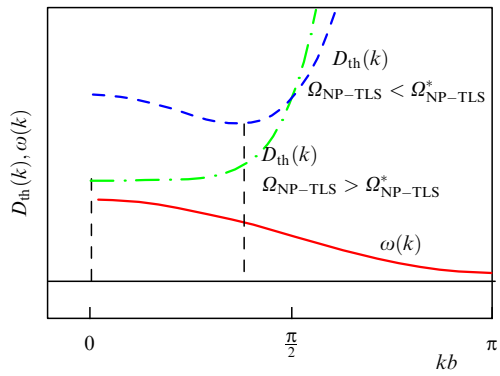

Figure 8. Dependence of the threshold pumping value on the wave vector k for $\Omega_{\mathrm{NP-TLS}} < \Omega^*_{\mathrm{NP-TLS}}$ (dashed curve) and $\Omega_{\mathrm{NP-TLS}} > \Omega^*_{\mathrm{NP-TLS}}$ (dot-and-dash curve). The solid curve depicts the $\omega(k)$ dependence.

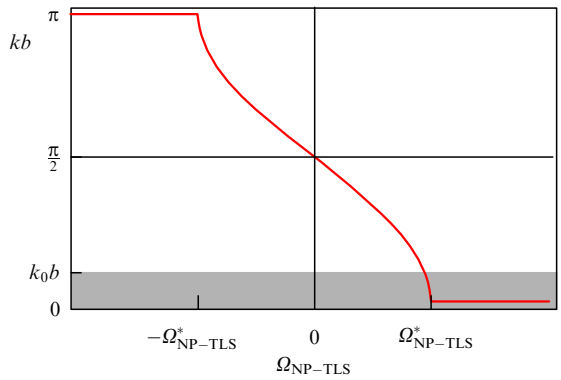

Figure 9. Dependence of the magnitude of a wave vector on the coupling constant between the neighboring NP and QD. The shaded domain corresponds to the leaky wave type solution.

Acknowledgments

The authors express their appreciation to J B Pendry for the critical discussion of this work. This research was supported in part by the Russian Foundation for Basic Research under grant Nos 10-02-92115 and 10-02-91750, by a PSC-CUNY

grant, and by the Dinastiya Foundation for Noncommercial Programs.

References

1. Bozhevolnyi S I (Ed.) *Plasmonic Nanoguides and Circuits* (Singapore: Pan Stanford Publ., 2009)
2. Chang D E et al. *Phys. Rev. Lett.* **97** 053002 (2006)
3. Gaponenko S V *Introduction to Nanophotonics* (Cambridge: Cambridge Univ. Press, 2010)
4. Martín-Cano D et al. *Nano Lett.* **10** 3129 (2010)
5. Plum E et al. *Opt. Express* **17** 8548 (2009)
6. Premaratne M, Agrawal G P *Light Propagation in Gain Media: Optical Amplifiers* (New York: Cambridge Univ. Press, 2011)
7. Protsenko I E et al. *J. Phys. Conf. Ser.* **107** 012010 (2008)
8. Protsenko I E et al. *Phys. Rev. A* **71** 063812 (2005)
9. Ridolfo A et al. *Phys. Rev. Lett.* **105** 263601 (2010)
10. Rosenthal A S, Ghannam T *Phys. Rev. A* **79** 043824 (2009)
11. Stockman M I *New J. Phys.* **10** 025031 (2008)
12. Stockman M I *J. Opt.* **12** 024004 (2010)
13. Wang Z M, Neogi A (Eds) *Nanoscale Photonics and Optoelectronics* (New York: Springer Science + Business Media, 2010)
14. Zheludev N I et al. *Nature Photon.* **2** 351 (2008)
15. Klimov V V *Usp. Fiz. Nauk* **178** 875 (2008) [*Phys. Usp.* **51** 839 (2008)]
16. Novotny L, Hecht B *Principles of Nano-Optics* (Cambridge: Cambridge Univ. Press, 2006) [Translated into Russian (Moscow: Fizmatlit, 2009)]
17. Maier S A *Plasmonics: Fundamentals and Applications* (New York: Springer, 2007) [Translated into Russian (Moscow – Izhevsk: RKhD, 2011)]
18. Sarychev A K, Shalaev V M *Elektrodinamika Metamaterialov* (Electrodynamics of Metamaterials) (Moscow: Nauchnyi Mir, 2011); *Electrodynamics of Metamaterials* (Singapore: World Scientific, 2007)
19. Shalaev V M, Kawata S (Eds) *Nanophotonics with Surface Plasmons* (Amsterdam: Elsevier, 2007)
20. Andrianov E S et al. *Opt. Lett.* **36** 4302 (2011)
21. Andrianov E S et al. *Opt. Express* **19** 24849 (2011)
22. Andrianov E S et al. *Phys. Rev. B* **85** 035405 (2012)
23. Lisyansky A A et al. *Phys. Rev. B* **84** 153409 (2011)
24. Andrianov E S et al. *Radiotekh. Elektron.* **56** 1501 (2011) [*J. Commun. Technol. Electron.* **56** 1471 (2011)]
25. Andrianov E S et al. *Radiotekh. Elektron.* **57** 114 (2012) [*J. Commun. Technol. Electron.* **57** 106 (2012)]
26. Berndt R, Gimzewski J K, Johansson P *Phys. Rev. Lett.* **67** 3796 (1991)
27. Blackie E J, Le Ru E C, Etchegoin P G *J. Am. Chem. Soc.* **131** 14466 (2009)
28. Le Ru E C et al. *J. Phys. Chem. C* **111** 13794 (2007)
29. Kneipp K, Moskovits M, Kneipp H (Eds) *Surface-Enhanced Raman Scattering: Physics and Applications* (Berlin: Springer, 2006)
30. Schlücker S (Ed.) *Surface Enhanced Raman Spectroscopy: Analytical, Biophysical and Life Science Applications* (Weinheim: Wiley-VCH, 2011)
31. Cai W, Shalaev V *Optical Metamaterials: Fundamentals and Applications* (New York: Springer, 2010)
32. Pendry J B *Phys. Rev. Lett.* **85** 3966 (2000)
33. Belov P A, Simovski C R, Ikonen P *Phys. Rev. B* **71** 193105 (2005)
34. Chen H et al. *Phys. Rev. Lett.* **99** 063903 (2007)
35. Cummer S A et al. *Phys. Rev. E* **74** 036621 (2006)
36. Leonhardt U *IEEE J. Sel. Top. Quantum Electron.* **9** 102 (2003)
37. Liu Z et al. *Science* **315** 1686 (2007)
38. Pendry J B, Schurig D, Smith D R *Science* **312** 1780 (2006)
39. Schurig D et al. *Science* **314** 977 (2006)
40. Yang J et al. *Opt. Express* **17** 19656 (2009)
41. Kolokolov A A, Skrotskii G V *Usp. Fiz. Nauk* **162** (12) 165 (1992) [*Sov. Phys. Usp.* **35** 1089 (1992)]
42. Vinogradov A P, Dorofeenko A V *Opt. Commun.* **256** 333 (2005)
43. Lagarkov A N et al. *Usp. Fiz. Nauk* **179** 1018 (2009) [*Phys. Usp.* **52** 959 (2009)]
44. Noginov M A et al. *Opt. Express* **16** 1385 (2008)
45. Noginov M A et al. *Opt. Lett.* **31** 3022 (2006)
46. Popov A K, Shalaev V M *Opt. Lett.* **31** 2169 (2006)
47. Anantha Ramakrishna S, Pendry J B *Phys. Rev. B* **67** 201101(R) (2003)
48. Sarychev A K, Pukhov A A, Tartakovsky G *PIERS Online* **3** 1264 (2007)
49. Sarychev A K, Tartakovsky G *Proc. SPIE* **6320** 63200A (2006)
50. Wuestner S et al. *Phys. Rev. Lett.* **105** 127401 (2010)
51. Yu Z et al. *Appl. Phys. Lett.* **92** 041117 (2008)
52. Shatrov A D *Radiotekh. Elektron.* **52** 909 (2007) [*J. Commun. Technol. Electron.* **52** 842 (2007)]
53. Shatrov A D *Radiotekh. Elektron.* **52** 1430 (2007) [*J. Commun. Technol. Electron.* **52** 1324 (2007)]
54. Bergman D J, Stockman M I *Phys. Rev. Lett.* **90** 027402 (2003)
55. Noginov M A et al. *Nature* **460** 1110 (2009)
56. Fang A, Koschny T, Soukoulis C M *J. Opt.* **12** 024013 (2010)
57. Fang A et al. *Phys. Rev. B* **79** 241104(R) (2009)
58. Gabitov I R, Kennedy B, Maimistov A I *IEEE J. Sel. Top. Quantum Electron.* **16** 401 (2010)
59. Bykov V P *Lazernaya Elektrodinamika: Elementarnye i Kogerentnye Protsessy pri Vzaimodeistvii Lazernogo Izlucheniya s Veshchestvom* (Laser Electrodynamics: Elementary and Coherent Processes in the Interaction of Laser Radiation with Matter) (Moscow: Fizmatlit, 2006)]
60. Klimov V V *Nanoplazmonika* (Nanoplasmonics) (Moscow: Fizmatlit, 2010)
61. Davis L C *Phys. Rev. B* **14** 5523 (1976)
62. Eguiluz A, Maradudin A A *Phys. Rev. B* **14** 5526 (1976)
63. Gramotnev D K, Bozhevolnyi S I *Nature Photon.* **4** 83 (2010)
64. Novikov I V, Maradudin A A *Phys. Rev. B* **66** 035403 (2002)
65. Hill M T et al. *Opt. Express* **17** 11107 (2009)
66. Zuev V S, Preprint No. 3 (Moscow: Lebedev Physical Institute, 2006)
67. Zuev V S, Zueva G Ya *Opt. Spektrosk.* **107** 648 (2009) [*Opt. Spectrosc.* **107** 614 (2009)]
68. Palik E D (Ed.) *Handbook of Optical Constants of Solids* (Orlando: Academic Press, 1985)
69. Muller A et al. *Appl. Phys. Lett.* **84** 981 (2004)
70. Scully M O, Zubairy M S *Quantum Optics* (Cambridge: Cambridge Univ. Press, 1997) [Translated into Russian (Moscow: Fizmatlit, 2003)]
71. Milonni P W *J. Mod. Opt.* **42** 1991 (1995)
72. Landau L D, Lifshitz E M, Pitaevskii L P *Elektrodinamika Sploshnykh Sred* (Electrodynamics of Continuous Media) (Moscow: Fizmatlit, 2003) [Translated into English (Oxford: Pergamon Press, 1984)]
73. Sarychev A K, Tartakovsky G *Phys. Rev. B* **75** 085436 (2007)
74. Pantell R H, Puthoff H E *Fundamentals of Quantum Electronics* (New York: Wiley, 1969) [Translated into Russian (Moscow: Mir, 1972)]
75. Li K et al. *Phys. Rev. B* **71** 115409 (2005)
76. Stietz F et al. *Phys. Rev. Lett.* **84** 5644 (2000)
77. Bayer M, Forchel A *Phys. Rev. B* **65** 041308(R) (2002)
78. Harbold J M et al. *Phys. Rev. B* **72** 195312 (2005)
79. Sosnowski T S et al. *Phys. Rev. B* **57** R9423 (1998)
80. Anishchenko V S, Astakhov V V, Vadivasova T E *Regulyarnye i Khaoticheskie Avtokolebaniya: Sinkhronizatsiya i Vliyanie Fluktuatsii* (Regular and Chaotic Self-Oscillations: Synchronization and the Effect of Fluctuations) (Dolgoprudnyi: Intellekt, 2009)
81. Kuznetsov A P, Kuznetsov S P, Ryskin N M *Nelineinye Kolebaniya* (Nonlinear Oscillations) (Moscow: Fizmatlit, 2002)
82. Pikovsky A, Rosenblum M, Kurths J *Synchronization: A Universal Concept in Nonlinear Sciences* (Cambridge: Cambridge Univ. Press, 2001) [Translated into Russian (Moscow: Tekhnosfera, 2003)]
83. Fedyanin D Yu, Arsenin A V *Opt. Express* **19** 12524 (2011)
84. Flynn R A et al. *Opt. Express* **19** 8954 (2011)
85. Vainshtein L A *Elektromagnitnye Volny* (Electromagnetic Waves) (Moscow: Radio i Svyaz', 1988)
86. Scott A *Nonlinear Science: Emergence and Dynamics of Coherent Structures* (Oxford: Oxford Univ. Press, 2003) [Translated into Russian (Moscow: Fizmatlit, 2007)]

PACS numbers: 33.50.Dq, 73.20.Mf, 78.20.Ek
DOI: 10.3367/UFNe.0182.201210k.1130

Using chiral nano-meta-particles to control chiral molecule radiation

V V Klimov, D V Guzatov

1. Introduction

Currently, owing to the development of nanotechnologies, new areas of optics have made their appearance — nanooptics and nanoplasmonics, whose subjects are the highly nontrivial properties of optical fields on the nanoscale and their practical applications [1, 2]. Among the most important advantages in this area is the capability of exerting effective control over the radiation of ordinary atoms and molecules with the help of nanoparticles [surface enhanced Raman scattering (SERS), surface enhanced fluorescence (SEF)] [3–6]. Interesting effects have also been discovered in the investigation of the influence of chiral nanoparticles or nanoparticles of metamaterials with a negative refractive index on the radiation of ordinary molecules [7, 8].

More complex optically active (chiral) molecules are of greater interest because they form the basis of life. This brings up the natural question: Is it possible to efficiently and arbitrarily control the radiation of chiral molecules and use this for various biomedical applications (for instance, for separating racemic mixtures)? We show in our paper that this control is possible if advantage is taken of nanoparticles made of metamaterials (see, for instance, Refs [9, 10]).

2. Chirality and optical activity

Chirality is the property of a system not to coincide with its mirror image under arbitrary rotations and translations [11]. It follows from this definition that, first, chirality is a geometric property of objects and, second, this property may be inherent only in spatial, i.e. three-dimensional, objects. The most important chiral objects are aminoacids and sugars which can exist, in principle, in the form of right or left enantiomers. However, of the utmost significance is the fact that the right enantiomers of aminoacids and the left enantiomers of sugars are not encountered in living nature. It is precisely this asymmetry that makes extremely important the optical investigations of these and kindred phenomena. The possibility of these investigations relies on the circumstance that chiral molecules quite often possess the property of optical activity, i.e. react to light with different polarizations in different ways. In particular, when linearly polarized light is incident on optically active molecules, its plane of polarization changes (rotates) and the degree of this rotation is defined by the factor

$$\frac{n_{\text{left}} - n_{\text{right}}}{n_{\text{left}} + n_{\text{right}}} \sim \frac{\text{molecular size}}{\text{wavelength}} \ll 1\,, \tag{1}$$

where n_{left} and n_{right} are the refractive indices for the left- and right-polarized waves.

The absorption of waves with different circular polarization is also different, and the degree of this difference is defined by the factor

$$\frac{A_{\text{left}} - A_{\text{right}}}{A_{\text{left}} + A_{\text{right}}} \sim \frac{\text{molecular size}}{\text{wavelength}} \ll 1\,, \tag{2}$$

where A_{left} and A_{right} are the absorption coefficients for the left- and right-polarized waves. Since the molecular size is usually small in comparison with optical wavelengths, the optical activity effects are quite weak. Despite this smallness, the effects of rotation of the polarization plane and circular dichroism enjoy wide application in the exploration of different conformations of biomolecules.

By applying the methods of nanooptics and nanoplasmonics, it is possible to significantly (by 4–6 orders of magnitude!) enhance these extremely weak effects by using nanostructured chiral metamaterials [12] or even the clusters of nonchiral nanoparticles [13].

Our aim is to learn to control precisely the *emission* of light by chiral molecules (and not the *absorption* of light) with the help of chiral nano-meta-particles (see below what this is).

3. Chiral molecules

To solve the problem of controling the light emission by chiral molecules requires, first of all, recognizing the difference between 'ordinary' and 'optically active' (chiral) molecules. Ordinary molecules are characterized only by the electric dipole moment, and their light–matter interaction Hamiltonian is of the form

$$H_{\text{int}} = -\mathbf{dE}\,, \tag{3}$$

where $\mathbf{d}$ is the dipole transition moment between the ground and excited states, and $\mathbf{E}$ is the electric field strength at the point of location of the molecule. This Hamiltonian does not permit describing the effects of optical activity in principle.

Chiral (optically active) molecules possess both electric and magnetic transition moments [14, 15]. In this case, when a spiral is considered as the model of a chiral molecule, for right molecules, in which the electric and magnetic transition moments are parallel, the Hamiltonian for their interaction with an electromagnetic field takes the form

$$H_{\text{int}} = -\mathbf{dE} - \mathbf{mH}\,, \tag{4}$$

while for left molecules, for which the electric and magnetic transition moments are antiparallel, the Hamiltonian for their interaction with an electromagnetic field is given by

$$H_{\text{int}} = -\mathbf{dE} + \mathbf{mH}\,. \tag{5}$$

In expressions (4) and (5), $\mathbf{d}$ and $\mathbf{m}$ are the dipole transition moments between the ground and excited states in the right molecule, and $\mathbf{E}$ and $\mathbf{H}$ are the strengths of the electromagnetic field at the point of its location.

4. Chiral nano-meta-particles

Controling the radiation of chiral molecules calls for the efficient 'mixing' of electric and magnetic fields, chiral nano-meta-particles being ideally suited for this purpose. In the simplest case, we may consider for such a particle a plasmon

V V Klimov Lebedev Physical Institute, Russian Academy of Sciences, Moscow, Russian Federation; Optical Nanodevices Ltd, Moscow, Russian Federation. E-mail: vklim@sci.lebedev.ru
D V Guzatov Yanka Kupala State University of Grodno, Grodno, Belarus

Uspekhi Fizicheskikh Nauk **182** (10) 1130 – 1135 (2012)
DOI: 10.3367/UFNr.0182.201210k.1130
Translated by E N Ragozin; edited by A Radzig

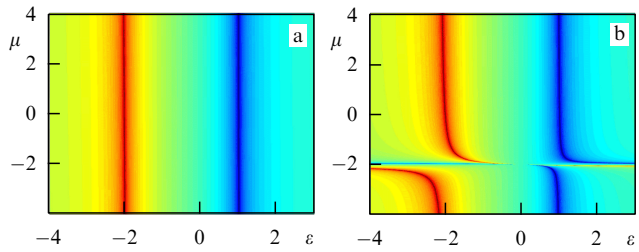

Figure 1. Chiral plasmon resonance in a spherical particle with $k_0 a = 0.1$: (a) $\chi = 0$, and (b) $\chi = 0.1$.

chiral nanoparticle, i.e., a layered nanoparticle (a nanodimension: a dimension shorter than the wavelength) whose core comprises gold, and the shell consists of natural sugar. In the general case, the constitutive equations of the substance of a chiral nano-meta-particle have the form [16]

$$\mathbf{D} = \varepsilon(\mathbf{E} + \eta \operatorname{rot} \mathbf{E}), \qquad \mathbf{B} = \mu(\mathbf{H} + \eta \operatorname{rot} \mathbf{H}), \tag{6}$$

where $\mathbf{D}$, $\mathbf{E}$ and $\mathbf{B}$, $\mathbf{H}$ are the induction and strength of electric and magnetic fields, respectively, ε, μ are the permittivity and permeability of the material of the chiral medium, and η is the chirality dimensional parameter. The chirality dimensionless parameter is conveniently introduced by the expression $\chi = \omega\eta/c$.

One can see from formulas (6) that, as in the case of optically active molecules [see expressions (4) and (5)], entangling of electric and magnetic phenomena occurs, and such nanoparticles would be expected to efficiently interact with chiral molecules. We note that the constitutive equations correspond to so-called chiral (bi-isotropic) media [17], to state it in more formal terms.

Even a small chirality of a nanoparticle leads to a significant change in its resonance optical properties. Figure 1 shows the dependence of the resonance properties of a chiral plasmon spherical nanoparticle on the permittivity and the permeability. Figure 1a corresponds to the case of a zero-chirality nano-meta-particle. As is evident from this figure, an ordinary plasmon resonance occurs at $\varepsilon \approx -2$, which is hardly dependent on the permeability of the nanoparticle. The situation becomes significantly different when the nanoparticle has an arbitrarily small admixture of chirality (Fig. 1b) because the interaction of electric and magnetic oscillations results in a significant change in the resonance structure, i.e., a chiral plasmon resonance appears. It is precisely the chiral plasmon resonance that makes it possible to exert efficient selective control over the radiation of chiral molecules.

5. Quantum theory of the radiation of a chiral molecule near a chiral nano-meta-sphere

As discussed in the Introduction, the rate of spontaneous emission depends significantly on the nanoenvironment, and in this section we shall consistently describe the quantum theory of spontaneous emission by a chiral molecule residing near a chiral nanoparticle [18].

Fermi's golden rule [19] is fully applicable in the chiral case, and the spontaneous relaxation probability can be described by the well-known expression

$$\Gamma = \frac{2\pi}{\hbar} \sum_{\text{final}} \left| \langle \text{initial} \,|H_{\text{int}}|\, \text{final} \rangle \right|^2 \rho(\omega), \tag{7}$$

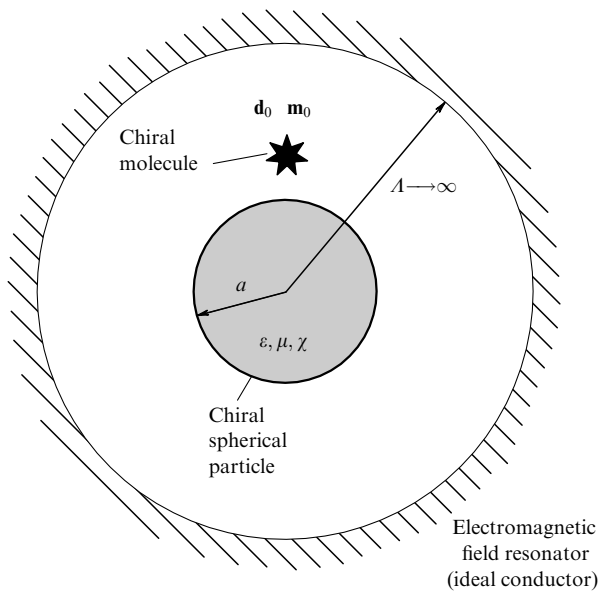

Figure 2. Geometry of electromagnetic field quantization in the presence of a chiral sphere.

where $\rho(\omega)$ is the density of final states, $H_{\text{int}} = -(\hat{\mathbf{d}}\hat{\mathbf{E}}(\mathbf{r}_0)) - (\hat{\mathbf{m}}\hat{\mathbf{H}}(\mathbf{r}_0))$ is the interaction Hamiltonian between the electromagnetic field and the chiral molecule, $\hat{\mathbf{d}} = e\hat{\mathbf{r}}$ and $\hat{\mathbf{m}} = -\mathrm{i}\hbar e/(2mc)\,(\hat{\mathbf{r}} \times \nabla)$ are the electric and magnetic dipole moment operators, and finally

$$\hat{\mathbf{E}}(\mathbf{r}) = \mathrm{i} \sum_s \frac{a_s \mathbf{e}(s,\mathbf{r}) - a_s^\dagger \mathbf{e}^*(s,\mathbf{r})}{\sqrt{2}},$$

$$\hat{\mathbf{H}}(\mathbf{r}) = \sum_s \frac{a_s \mathbf{h}(s,\mathbf{r}) + a_s^\dagger \mathbf{h}^*(s,\mathbf{r})}{\sqrt{2}}$$

are the quantized electromagnetic field operators (index s numbers the modes).

By and large, the quantization of the electromagnetic field reduces to finding the eigenmodes $\mathbf{e}(s,\mathbf{r})$, $\mathbf{h}(s,\mathbf{r})$ of the system, and these modes are termed photons. In our case, unfortunately, the ordinary notions of photons (TE and TM modes) are inapplicable and the entire quantization procedure is to be constructed anew. To do this, we assume that our system, a molecule and a nanoparticle, is placed in an infinitely large spherical resonator with an ideally conducting wall (Fig. 2). After this, the photon mode inside the sphere may be sought in the form of an expansion in terms of vector spherical harmonics [20]:

$$\mathbf{e}_{mn}(\mathbf{r}) = A^{\mathrm{L}}_{mn}(\mathbf{N}\boldsymbol{\psi}^{\mathrm{L}}_{mn} + \mathbf{M}\boldsymbol{\psi}^{\mathrm{L}}_{mn}) + A^{\mathrm{R}}_{mn}(\mathbf{N}\boldsymbol{\psi}^{\mathrm{R}}_{mn} - \mathbf{M}\boldsymbol{\psi}^{\mathrm{R}}_{mn}), \tag{8}$$

with combinations of TE and TM harmonics entering into this expression, and indices L and R pertaining to left- and right-polarized plane waves in free space with respective wave numbers

$$k_{\mathrm{L}} = \frac{k_0\sqrt{\varepsilon\mu}}{1 - \chi\sqrt{\varepsilon\mu}}, \qquad k_{\mathrm{R}} = \frac{k_0\sqrt{\varepsilon\mu}}{1 + \chi\sqrt{\varepsilon\mu}}.$$

The photon mode outside the particle is sought in the form of a combination of diverging and converging spherical TE and TM waves [20]:

$$\mathbf{e}_{mn}(\mathbf{r}) = C^{(1)}_{mn}\mathbf{N}\boldsymbol{\zeta}^{(1)}_{mn} + C^{(2)}_{mn}\mathbf{N}\boldsymbol{\zeta}^{(2)}_{mn} + D^{(1)}_{mn}\mathbf{M}\boldsymbol{\zeta}^{(1)}_{mn} + D^{(2)}_{mn}\mathbf{M}\boldsymbol{\zeta}^{(2)}_{mn}. \tag{9}$$

By imposing the continuity boundary conditions for the tangential field strength components and applying normalization to one photon throughout the space, it is possible to derive explicit expressions for all coefficients entering into expressions (8) and (9) [18]. The resultant dispersion equation has two solutions which correspond to two types of photons. These photon types will be referred to as A and B. For $\chi = 0$, the A type photons reduce to TM photons, and the B type photons reduce to TE photons. The final state density for photons of any type, $\rho(\omega) = \Lambda/(\pi\hbar c)$, is independent, in accordance with the Courant theorem [21], of the presence of finite-sized particles.

By using the derived expressions and writing the molecular transition matrix elements as $\mathbf{d}_0 = \langle e|\hat{\mathbf{d}}|g\rangle$ and $-\mathrm{i}\mathbf{m}_0 = \langle e|\hat{\mathbf{m}}|g\rangle$, the spontaneous emission rate (7) for an arbitrary chiral molecule near an arbitrary bi-isotropic sphere may be represented as the sum of decay rates to A- and B-type photons. For instance, for the decay rate to A type photons we have

$$\gamma_{eg}^{\mathrm{A}} = \gamma_{eg}^{\mathrm{A},-1} + \gamma_{eg}^{\mathrm{A},1} + \gamma_{eg}^{\mathrm{A},0}\,, \tag{10}$$

where

$$\begin{aligned}\gamma_{eg}^{\mathrm{A},-1} = {} & \frac{k_0}{2\hbar r_0^2}\sum_{n=1}^{\infty}\frac{2n+1}{1+|O_n|^2} \\ & \times\Big|(d_{0x}-\mathrm{i}d_{0y})\big(\psi_n'(k_0r_0)+T_n^{\mathrm{A}}\zeta_n^{(1)\prime}(k_0r_0)\big) \\ & - O_n(d_{0y}+\mathrm{i}d_{0x})\big(\psi_n(k_0r_0)+L_n^{\mathrm{A}}\zeta_n^{(1)}(k_0r_0)\big) \\ & + O_n(m_{0x}-\mathrm{i}m_{0y})\big(\psi_n'(k_0r_0)+L_n^{\mathrm{A}}\zeta_n^{(1)\prime}(k_0r_0)\big) \\ & - (m_{0y}+\mathrm{i}m_{0x})\big(\psi_n(k_0r_0)+T_n^{\mathrm{A}}\zeta_n^{(1)}(k_0r_0)\big)\Big|^2\,,\end{aligned} \tag{11}$$

$$\begin{aligned}\gamma_{eg}^{\mathrm{A},1} = {} & \frac{k_0}{2\hbar r_0^2}\sum_{n=1}^{\infty}\frac{2n+1}{1+|O_n|^2} \\ & \times\Big|O_n(d_{0y}-\mathrm{i}d_{0x})\big(\psi_n(k_0r_0)+L_n^{\mathrm{A}}\zeta_n^{(1)}(k_0r_0)\big) \\ & - (d_{0x}+\mathrm{i}d_{0y})\big(\psi_n'(k_0r_0)+T_n^{\mathrm{A}}\zeta_n^{(1)\prime}(k_0r_0)\big) \\ & + (m_{0y}-\mathrm{i}m_{0x})\big(\psi_n(k_0r_0)+T_n^{\mathrm{A}}\zeta_n^{(1)}(k_0r_0)\big) \\ & - O_n(m_{0x}+\mathrm{i}m_{0y})\big(\psi_n'(k_0r_0)+L_n^{\mathrm{A}}\zeta_n^{(1)\prime}(k_0r_0)\big)\Big|^2\,,\end{aligned} \tag{12}$$

$$\begin{aligned}\gamma_{eg}^{\mathrm{A},0} = {} & \frac{2}{\hbar k_0 r_0^4}\sum_{n=1}^{\infty}\frac{(2n+1)n(n+1)}{1+|O_n|^2} \\ & \times\Big|d_{0z}\big(\psi_n(k_0r_0)+T_n^{\mathrm{A}}\zeta_n^{(1)}(k_0r_0)\big) \\ & + O_n m_{0z}\big(\psi_n(k_0r_0)+L_n^{\mathrm{A}}\zeta_n^{(1)}(k_0r_0)\big)\Big|^2\,,\end{aligned} \tag{13}$$

and T_n^{A}, L_n^{A}, and O_n are some coefficients which are expressed in terms of the Bessel functions and which depend only on the properties of the sphere [18]. Similar expressions are obtained for the rate of decay to B photons [18].

6. Analysis of results and illustrations

Expressions (11)–(13) virtually exhaust the problem of spontaneous radiation by an arbitrary molecule residing near a chiral sphere of arbitrary composition and size. Unfortunately, these expressions are cumbersome, which hinders their understanding and interpretation. In the most interesting case of a nanosphere, expressions (11)–(13) may be simplified. However, instead of the formal derivation of asymptotics, below we consider the spontaneous emission by chiral molecules, which are located near a chiral nano-meta-particle, in the framework of a quasistatic (and quasiclassical) approximation [22]. As will be clear, this more physical approach agrees nicely with the exact solution (11)–(13) and permits a complete understanding of the physics of the processes.

The near fields produced by the molecule, which is described by oscillating electric and magnetic dipole moments with amplitudes $\mathbf{d}_0$ and $-\mathrm{i}\mathbf{m}_0$, have the well-known form

$$\mathbf{E}_0 = \frac{3\mathbf{r}(\mathbf{r}\mathbf{d}_0) - r^2\mathbf{d}_0}{r^5}\,, \qquad \mathbf{H}_0 = -\frac{\mathrm{i}\big(3\mathbf{r}(\mathbf{r}\mathbf{m}_0) - r^2\mathbf{m}_0\big)}{r^5}\,, \tag{14}$$

where $\mathbf{r}$ is the radius vector emanating from the sphere center to the point of observation. In expressions (14) and further, the factor of monochromatic time dependence is omitted.

The near fields (14) induce dipole moments in the nanoparticle:

$$\begin{aligned}\delta\mathbf{d} &= \alpha_{EE}\mathbf{E}_0(\mathbf{r}_0) + \alpha_{EH}\mathbf{H}_0(\mathbf{r}_0)\,, \\ \delta\mathbf{m} &= \alpha_{HE}\mathbf{E}_0(\mathbf{r}_0) + \alpha_{HH}\mathbf{H}_0(\mathbf{r}_0)\,,\end{aligned} \tag{15}$$

where the electromagnetic polarizabilities of the chiral sphere are of the form

$$\begin{aligned}\alpha_{EE} &= a^3\,\frac{(\varepsilon-1)(\mu+2)+2\varepsilon\mu\chi^2}{(\varepsilon+2)(\mu+2)-4\varepsilon\mu\chi^2}\,, \\ \alpha_{EH} &= a^3\,\frac{3\chi\varepsilon\mu\mathrm{i}}{(\varepsilon+2)(\mu+2)-4\varepsilon\mu\chi^2}\,, \\ \alpha_{HH} &= \alpha_{EE}(\varepsilon\leftrightarrow\mu)\,, \qquad \alpha_{HE} = -\alpha_{EH}\,.\end{aligned} \tag{16}$$

If it is additionally assumed that the molecule–nanoparticle distance is small in comparison with the wavelength, and the radiation intensity of the particle + molecule system is described by the expression

$$\Gamma \propto |\mathbf{d}_0 + \delta\mathbf{d}|^2 + |-\mathrm{i}\mathbf{m}_0 + \delta\mathbf{m}|^2\,, \tag{17}$$

in which the interference between the radiations of the electric and magnetic dipoles does not take place owing to the smallness of phase incursion. Substituting expressions (15) into expression (17) yields

$$\begin{aligned}\Gamma \propto {} & \left|\mathbf{d}_0 + \frac{\alpha_{EE}}{r_0^3}\big(3\mathbf{n}(\mathbf{n}\mathbf{d}_0)-\mathbf{d}_0\big) - \frac{\mathrm{i}\alpha_{EH}}{r_0^3}\big(3\mathbf{n}(\mathbf{n}\mathbf{m}_0)-\mathbf{m}_0\big)\right|^2 \\ & + \left|\mathbf{m}_0 + \frac{\mathrm{i}\alpha_{HE}}{r_0^3}\big(3\mathbf{n}(\mathbf{n}\mathbf{d}_0)-\mathbf{d}_0\big) + \frac{\alpha_{HH}}{r_0^3}\big(3\mathbf{n}(\mathbf{n}\mathbf{m}_0)-\mathbf{m}_0\big)\right|^2.\end{aligned} \tag{18}$$

When the orientation of the molecules is not fixed, as is often the case in practice, we must perform averaging over it to obtain

$$\begin{aligned}\Gamma_{\mathrm{eff}} = {} & \frac{4k_0^3|\mathbf{d}_0|^2}{3\hbar}\left\{1 + \frac{2}{r_0^6}|\alpha_{EE} - \mathrm{i}\xi\alpha_{EH}|^2 + |\xi|^2\right. \\ & \left. + \frac{2}{r_0^6}|\mathrm{i}\alpha_{HE} + \xi\alpha_{HH}|^2\right\}\,,\end{aligned} \tag{19}$$

where $\mathbf{m}_0 = \xi\mathbf{d}_0$.

The results of calculations in the framework of quantum electrodynamics (QED) and in the quasistatic approximation

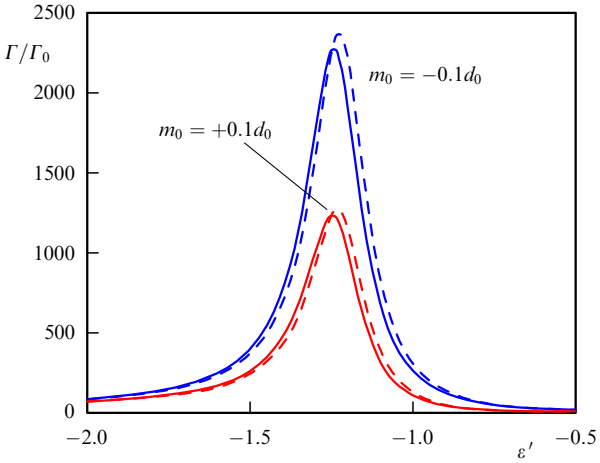

Figure 3. Comparison of the results of calculating the spontaneous emission rate for a chiral molecule in the framework of QED and in the quasistatic approximation. The molecule is located near the surface of a chiral spherical nanoparticle with $\varepsilon = \varepsilon' + \mathrm{i}0.1$, $\mu = -1.6$, $\chi = 0.2$, and $k_0 a = 0.1$. The molecule is radially oriented.

(19) are compared in Fig. 3. One can see from the figure that the results of this simple theory are in perfect agreement with the exact QED calculation [see expressions (11)–(13)] for nanoparticles. The simplicity of interpreting this theory permits determining the explicit conditions whereat the radiation of a chiral molecule of one chirality or other will be suppressed. Realizing this requires that

(i) the system have a chiral plasmon resonance

$$(\varepsilon + 2)(\mu + 2) - 4\varepsilon\mu\chi^2 = 0 \tag{20}$$

(this permits enhancing the magnetic fields);

(ii) the electric moment induced in the nanoparticle be equal to zero:

$$d_0\alpha_{EE} - \mathrm{i}m_0\alpha_{EH} = 0\,. \tag{21}$$

whence, follows the discrimination condition

$$\mu^* \to -\frac{2d_0}{d_0 + 2m_0\chi}\,, \qquad \varepsilon^* \to -\frac{2m_0}{m_0 + 2d_0\chi}\,, \tag{22}$$

i.e., the chiral molecule radiation will be suppressed for these μ and ε. At the same time, the radiation from a molecule of opposite chirality ($m_0 \to -m_0$) located near the nanoparticle with parameters (22) will not be suppressed!

To illustrate this effect, Fig. 4 shows the rate of spontaneous emission by the left-hand chiral molecule and its ratio to the rate of spontaneous emission by the right-hand chiral molecule. One can see from this figure that the radiation by the right-hand molecule is almost suppressed, when condition (22) is fulfilled (in this case, when $\varepsilon \approx -0.4$ and $\mu \approx -2$, which corresponds to a metamaterial with a negative refractive index [23]), while the radiation by the left-hand molecule is enhanced by the chiral plasmon resonance. As a result, the decay rate for the left-hand molecule is more than 10 times higher than the decay rate for the right-hand molecule. We emphasize that such chiral metamaterials with a negative refractive index are quite realistic [24].

When it is required to suppress the radiation of the left-hand molecules and enhance the radiation of the right-hand ones, in accordance with condition (22) the nanoparticle metamaterial must have a positive permittivity and a negative permeability. Suchlike metamaterials are also quite possible [9, 10].

7. Applications of the effects discovered

Once we have theoretically shown that it is possible to suppress the radiation of some enantiomers and enhance the radiation of other ones by selecting the parameters of a chiral nanoparticle, many prospects open up for the application of this effect.

First of all, the effect discovered may be employed in the scanning microscope investigation of samples in which one type of enantiomers prevails, and so there is no way to discover and add up by ordinary methods the small amount of the enantiomer of opposite chirality. However, when a particle (Fig. 5), whose material is selected in conformity with conditions (22) so as to suppress the radiation of the bulk of unwanted molecules, is placed on the tip of a scanning microscope, only the sought-after molecules will come into the field of view of the microscope (the quest for extra-terrestrial life, bioterrorist attacks, etc.).

Of even greater importance is the application of the theoretical findings to the purely optical separation of racemic mixtures of biomolecules (Fig. 6). Such mixtures emerge, inter alia, in the chemical synthesis of medicines. However, only one specific enantiomer is required to achieve the correct action. The chemical separation methods in use

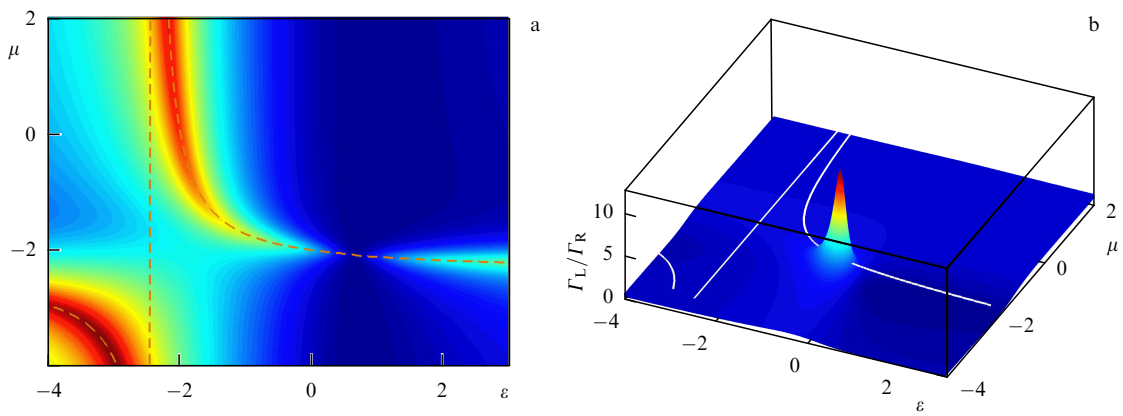

Figure 4. Rate Γ_L/Γ_0 of spontaneous emission by a left-hand molecule (a) and its ratio Γ_L/Γ_R to the rate of spontaneous emission by a right-hand molecule (b). The molecules are located near a chiral nano-meta-particle with $k_0 a = 0.1$, $\chi = 0.2$, $\xi = m_{0z}/d_{0z} = 0.1$, and $\varepsilon'' = 0.1$.

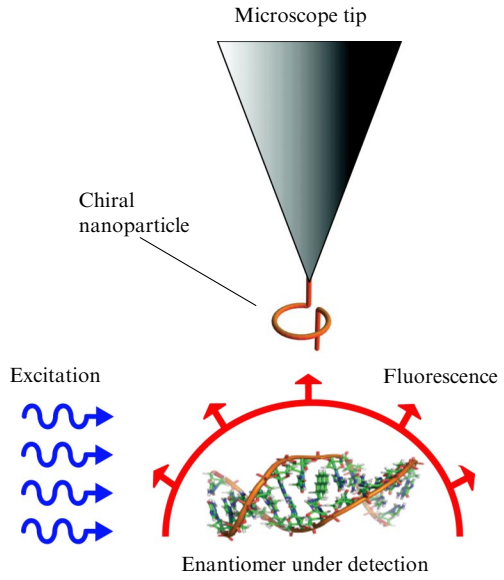

Figure 5. Detection of separate molecules of a given chirality.

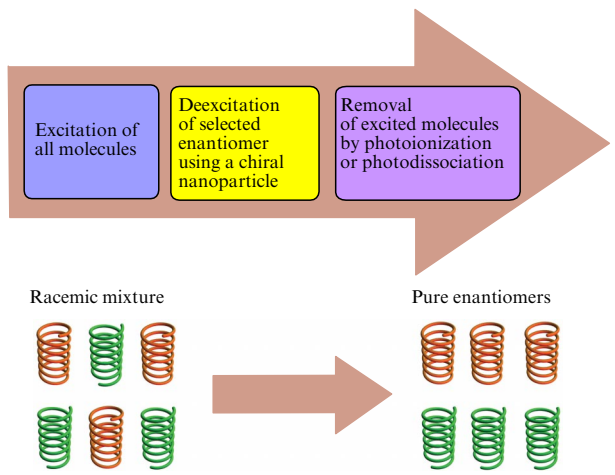

Figure 6. Separation of racemic mixtures of biomolecules.

today are complicated and expensive, and the development of a purely optical method for the separation of enantiomers is, therefore, quite appealing. The findings made above permit, at least in principle, doing this. The schematic of operation of a purely optical facility for enantiomer separation is illustrated in Fig. 6. In one way or another, the synthesized molecules are excited in a chamber, whose surface is covered by nanoparticles corresponding to condition (22). The enantiomers of one type (say, the 'right' ones) rapidly change to the ground state, while the enantiomers of the other type (the 'left' ones) remain in the excited state. By applying an ionizing radiation pulse, it is possible to remove the ionized molecules by an electric field, with the result that only the desired enantiomers will remain in the reaction chamber. It is significant that this synthesis technique is not attended by contamination from by-product chemicals required in the separation by chemical methods.

8. Conclusion

Thus, the problem of describing the spontaneous emission by chiral molecules located near a chiral sphere of arbitrary composition was analytically solved in the framework of QED, as well as in the quasistatic approximation.

As shown above, when a chiral particle has a negative refractive index or a negative permeability, the radiation of nearby right and left molecules may be significantly different. We emphasize that these results are general and are not restricted to the case of only one nanoparticle. It has already been found that the clusters of chiral nano-meta-particles show even greater promise for controling the radiation emitted by enantiomers [25].

These findings open the way to a purely optical separation of drug enantiomers.

Acknowledgments

This work was supported by the Russian Foundation for Basic Research under grant Nos 11-02-91065, 11-02-92002, 11-02-01272, 12-02-90014, and 12-0290417), the Belarussian Republican Foundation for Basic Research under grant No. F12R-006), the Programs of the Presidium of the Russian Academy of Sciences, and the Development Foundation of the Center for Development and Commercialization of New Technology (Skolkovo).

References

1. Novotny L, Hecht B *Principles of Nano-Optics* (Cambridge: Cambridge Univ. Press, 2006) [Translated into Russian (Moscow: Fizmatlit, 2009)]
2. Klimov V V *Nanoplazmonika* (Nanoplasmonics) (Moscow: Fizmatlit, 2010)
3. Klimov V V *Usp. Fiz. Nauk* **173** 1008 (2003) [*Phys. Usp.* **46** 979 (2003)]
4. Kneipp K, Moskovits M, Kneipp H (Eds) *Surface-Enhanced Raman Scattering*: *Physics and Applications* (Berlin: Springer, 2006)
5. Lakowicz J R et al. *J. Phys. D* **36** R240 (2003)
6. Manno D et al. *Nanotechnology* **21** 165502 (2010)
7. Lakhtakia A, Varadan V K, Varadan V V *J. Phys. D* **23** 481 (1990)
8. Klimov V V *Opt. Commun.* **211** 183 (2002)
9. Cai W, Shalaev V *Optical Metamaterials*: *Fundamentals and Applications* (New York: Springer, 2010)
10. Noginov M A, Podolskiy V A (Eds) *Tutorials in Metamaterials* (Boca Raton, FL: Taylor & Francis, 2012)
11. Kelvin W T (Lord) *Baltimore Lectures on Molecular Dynamics and the Wave Theory of Light* (London: C.J. Clay and Sons, 1904)
12. Hendry E et al. *Nature Nanotechnol.* **5** 783 (2010)
13. Govorov A O et al. *Nano Lett.* **10** 1374 (2010)
14. Rosenfeld L *Z. Phys.* **52** 161 (1929)
15. Barron L D *Molecular Light Scattering and Optical Activity* (Cambridge: Cambridge Univ. Press, 1982)
16. Bokut' B V, Serdyukov A N, Fedorov F I *Kristallogr.* **15** 1002 (1970) [*Sov. Phys. Crystallogr.* **15** 871 (1971)]
17. Lindell I V et al. *Electromagnetic Waves in Chiral and Bi-isotropic Media* (Boston: Artech House, 1994)
18. Guzatov D V, Klimov V V *New J. Phys.* **14** 123000 (2012)
19. Fermi E *Rev. Mod. Phys.* **4** 87 (1932)
20. Stratton J A *Electromagnetic Theory* (New York: McGraw-Hill, 1941) [Translated into Russian (Moscow – Leningrad: Gostekhizdat, 1948)]
21. Courant R, Hilbert D *Methoden der mathematischen Physik* (Methods of Mathematical Physics) (Berlin: J. Springer, 1931) [Translated into English (New York: Interscience Publ., 1989); Translated into Russian: Vol. 1 (Moscow – Leningrad: Gos. Tekh.-Teoretich. Izd., 1933) pp. 420, 421]
22. Klimov V V, Guzatov D V, Ducloy M *Europhysics Lett.* **97** 47004 (2012)
23. Veselago V G *Usp. Fiz. Nauk* **92** 517 (1967) [*Sov. Phys. Usp.* **10** 509 (1968)]
24. Kwon D-H et al. *Opt. Express* **16** 11822 (2008)
25. Guzatov D V, Klimov V V, Zabkov I V, Pavlov A A "Optical properties of a chiral nanoantenna and their influence on radiation of chiral molecules" (to be published)